March 2011

Design and Analysis of Subsystems for a CubeSat Mission

Andrew A. Oliva
Worcester Polytechnic Institute

Gregory Paul Schaalman
Worcester Polytechnic Institute

Simone Loretta Staley
Worcester Polytechnic Institute

Project Number: NAG-1002

Design and Analysis of Subsystems for a CubeSat Mission

A Major Qualifying Project Report

Submitted to the Faculty

of the

WORCESTER POLYTECHNIC INSTITUTE

in partial fulfillment of the requirements for the

Degree of Bachelor of Science

in Mechanical Engineering

by

Andrew Oliva

Gregory Schaalman

Simone Staley

March 15, 2011

Approved:

Professor Nikolaos A. Gatsonis, Advisor

Mechanical Engineering Department, WPI

Abstract

The project addresses the science payload and performs thermal and spacecraft charging analysis of a three-unit CubeSat under design. An infrared spectrometer and a magnetometer are selected for the circular 680-km polar CubeSat mission. Thermal analysis using SolidWorks provides the CubeSat temperature distribution under anticipated ambient and internal heat fluxes. To achieve the design temperatures thermal control is recommended with coatings and internal insulation. Charging analysis is performed using the Spacecraft Plasma Interaction System (SPIS) software under anticipated ambient plasma conditions and shows no adverse impacts. Electromagnetic interference due to the onboard propulsion solenoids is assessed using COMSOL. The analysis guides the design of a 10-cm magnetometer boom.

Acknowledgments

We would like to thank Professor John Blandino for his guidance and experience throughout the course of our MQP. Professor Blandino was a driving influence during all Systems Engineering Meetings, and he aided all of us in both our short-term individual efforts and our long-term project goals.

We would like to thank Professor Michael Demetriou for his continuous presence and guidance during the course of our project. We met with Professor Demitriou and his team multiple times per week over the course of this project, and their efforts were integral to our overall success.

We would like to thank Professor Blandino's CubeSat Design MQP students, Keith Cote, Jason Gabriel, Brijen Patel, Nick Ridley, Steve Tetreault, and Zach Taillefer, as well as Professor Demitriou's CubeSat Design MQP students, Andrew Bigelow and Cyle Hawkins, for their continuous teamwork and cooperation over the course of this project. Every teammate made contributions to the efforts of our common CubeSat team goals, and without them we would not have accomplished so much.

Finally, we would especially like to thank our advisor, Professor Nikolaos Gatsonis, for his support, guidance, and criticism throughout the MQP process. Professor Gatsonis played both the part of a strict boss and the part of an encouraging Professor, pushing us to be both confident in our work and open to suggestion for improvements. His comments and questions were always helpful, and his teamwork was indispensible.

Table of Contents

Authorship

	Writing	Editing
1.1: Overview	AO GS SS	GS
1.2: Literature Review	AO GS SS	GS
1.2.1: CubeSat Science and Mission Literature Review	GS SS	GS SS
1.2.2: Thermal and Environmental Literature Review	AO GS	AO GS
1.3: Objectives and Methods	AO GS	GS
1.3.1: Scientific Payload Design Objectives and Methods	GS SS	GS
1.3.2: Thermal Control Subsystem Design and Analysis Objectives and Methods	GS	GS
1.3.3: Space Environment Analysis and Design Objectives and Methods	AO	GS
1.3.4: Magnetometer Selection and Boom Design Objectives and Methods	GS	GS
Chapter 2: Scientific Payload Design	SS	GS SS
2.1: Scientific Instrument Selection	SS	GS SS
2.2: Orbital Elements	GS SS	GS SS
2.3: Ground Coverage	SS	GS SS
2.4: Data Processing and Analysis	SS	GS SS
2.5: On-Board Computer Interface	SS	GS SS
2.6: Power Interface	SS	GS SS
2.7: Structural Interface	SS	GS SS
2.8: Thermal and Environmental Requirements	SS	GS SS
Chapter 3: Thermal Control Subsystem Design and Analysis	GS	GS
3.1: Determining the Allowable Temperature Range	GS	GS
3.2: Determining Hot and Cold Cases	GS	GS
3.3: Relevant Equations of Heat Transfer	GS	GS
3.4: Baseline Temperature Analysis	GS	GS
3.5: Temperature Simulations in SolidWorks	GS	GS
3.5.1: Hot Case (Daylight)	GS	GS
3.5.2: Cold Case (Eclipse)	GS	GS
3.6: Thermal Control Subsystem Conclusions	GS	GS
4.1: Spacecraft Charging	AO	AO GS
4.1.1: Spacecraft Charging Modeling	AO	AO GS
4.1.2: Spacecraft Charging Software Analysis	AO	AO GS
4.1.3: Spacecraft Charging Simulation Results	AO	AO GS
4.2: Electromagnetic Interference Analysis	AO	AO GS
4.2.1 Modeling of Induced Magnetic Fields	AO	AO GS
4.2.2 EMI Software Evaluation	AO	AO GS
4.2.3: Expected Environment	AO	AO GS
4.2.4: EMI Results	AO	AO GS

Table of Figures

Table of Tables

Commonly Used Acronyms

ADCS……Attitude Determination and Controls Subsystem

AIRS……...…Argus 1000 Infrared Spectrometer

CAD……Computer-Aided Design

CMOS……Complementary Metal-Oxide Semiconductor

COTS……..……..Commercial-off-the-Shelf

CPU…….Central Processing Unit

EMI...……...……Electromagnetic Interference

GPS……..……Global Positioning System

IR……...Infrared

IRI……....International Reference Ionsphere

LEO……Low-Earth Orbit

MF…….Magnetic Field

MLI……Multi-Layer Insulation

OBC……..On-Board Computer

SEG……...Systems Engineering Group

SPIS……...Spacecraft Plasma Interaction System

STK……Satellite Tool Kit

WPI……..Worcester Polytechnic Institute

Chapter 1: Introduction

1.1: Overview

In 1999 California Polytechnic State University, San Luis Obispo, and Stanford University's Space Systems Development Lab started the CubeSat program with the goal of allowing people, universities, and companies the opportunity to access space. A standard one unit CubeSat is a 10cm cube that can weigh up to 1 kg; two and three unit versions are also permissible. The regulations on size and configuration also standardize the deployment interfacing system for the CubeSats by integrating four rails along the corners to specific sizes and lengths. The CubeSat program also provides the participants with the necessary documents and export licenses for launching their satellite into space. As of 2011, there are over 60 participants, universities and companies in the CubeSat program, some of which have launched more than one CubeSat. These participants come from all over the world, from places such as Japan, the US, Germany, and Switzerland. The CubeSat program has proven to be a reliable, practical and cost-effective program that allows launch opportunities to everyone.[1]

This project marks WPI's first foray into the CubeSat program. The entire CubeSat team consists of 11 Aerospace Engineering students divided into subsystem teams. The subsystem teams are:

1. Payload, Thermal, and Environmental Design.
2. Structural, Power, and Propulsion Design.
3. Attitude Determination, Control, and Computing Design.

Our team was in charge of designing a scientific payload for our proposed flight option CubeSat, and also with designing thermal and environmental control subsystems. In addition to

working on our own tasks, all three subsystem teams engaged in weekly System Engineering Group (SEG) meetings. During these SEG meetings, subsystem teams compared progress in their respective areas and communicated any requirements, questions, or results to other teams. In this way, all three teams worked on separate tasks towards one common project goal; designing a CubeSat that could be constructed and launched into space. Our team's specific goals are to:

1. Select a compatible scientific payload and design scientific mission requirements for the chosen payload. This information must be conveyed properly to all other subsystem teams, including supplying pointing requirements for proper data collection and interfacing needs for completely integrating the payload into the CubeSat.
2. Determine the allowable temperature range for the CubeSat during flight operations. The CubeSat's thermal environment during orbit must be predicted and analyzed to determine thermal effects and concerns. The thermal control subsystem must create and maintain a stable thermal environment for the operation of each subsystem's components.
3. Analyze the expected orbital trajectory for environmental effects and concerns. Identify what threat the ambient orbital environment poses to the CubeSat subsystems and create an appropriate environment for the fully functional operation of each subsystem's components.

1.2: Literature Review

Before embarking on our own project, we reviewed team documents and official publications of previously designed CubeSats to familiarize ourselves with the challenges and considerations of the CubeSat design process. Our review is divided into two sections; science and mission review, and thermal and environmental review. We found that while many teams kept extensive records of payload design considerations and final selections, there was a limited amount of thermal and environmental design material available. We have summarized some of our findings on the most well-documented CubeSat missions and subsystems in the following chapter.

1.2.1: CubeSat Science and Mission Literature Review

Table 1.1, shown below, contains a list of CubeSats that launched before July 2009 along with their basic orbital elements. The table also includes the launch vehicles utilized for each group launched. The data clearly indicates that majority of the past CubeSats chose a midrange altitude and an inclination of 98 degrees. The combination of these two orbital parameters creates a sun synchronous orbit, which is desirable for many reasons, including consistent lighting for picture taking, increased power production from solar cells (which either minimized or completely eliminated the need for a battery) due to limited eclipse time, and periodic orbital positioning for downlinks and uplinks.

General				Orbital Parameters	
Date	**Launch Vehicle**	**CubeSat**	**Developer**	**Inclination**	**Altitude**
Jun-03	Eurockot	Aau Cubesat	Aalborg Univ.	98.7 Deg	820km
		DTUsat-1	Technical Univ. of Denmark	98.7 Deg	820km
		CanX-1	Univ. of Toronto Inst. for Aero. Studies	98.7 Deg	820km
		Cute-1	Tokyo Institute of Technology	98.7 Deg	820km
		XI-IV	University of Tokyo	98.7 Deg	686km
		QuakeSat	Stanford Univ. and Quakefinder	98.7 Deg	820km
Oct-05	SSETI Express	Ncube-2	Norwegian Univ. of Science and Tech.	98.7 Deg	686km
		XI-V	Univ. of Tokyo	98.7 Deg	686km
		UWE-1	Univ. of Wurzburg	98.7 Deg	686km
Feb-06	M-V-8	Cute-1.7+APD	Tokyo Institute of Technology	98.7 Deg	750km
Jul-06	Dnepr (Launch Failed)	AeroCube-1	The Aerospace Corporation	97.43 Deg	600km
		CP1	Cal Poly, SLO	97.43 Deg	600km
		CP2	Cal Poly, SLO	97.43 Deg	600km
		ICEcube-1	Cornell University	97.43 Deg	600km
		ICEcube-2	Cornell University	97.43 Deg	600km
		ION	University of Illinois	97.43 Deg	600km
		HAUSAT 1	Hankuk Aviation University	97.43 Deg	600km
		KUTEsat	University of Kansas	97.43 Deg	600km
		MEROPE	Montana State University	97.43 Deg	600km
		NCUBE-1	Norwegian Univ. of Science and Tech.	97.43 Deg	600km
		RINCON	Univ. of Arizona	97.43 Deg	600km
		SACRED	Univ. of Arizona	97.43 Deg	600km
		SEEDS	Nihon University	97.43 Deg	600km
		Voyager	Univ. of Hawaii	97.43 Deg	600km
Dec-06	Minotaur 1	GeneSat-1	NASA Ames Research Center	40.5 Deg	460 km
Apr-07	Dnepr	CSTB1	The Boeing Company	98 Deg	700km
		AeroCube-2	The Aerospace Corporation	98 Deg	700km
		CP3	Cal Poly, SLO	98 Deg	700km
		CP4	Cal Poly, SLO	98 Deg	700km
		Libertad-1	Univ. Sergio Arboleda	98 Deg	700km
		CAPE1	Univ. of Louisiana	98 Deg	700km
		MAST	Tethers Unlimited, Inc.	98 Deg	700km
Apr-08	PSLV-C9	COMPASS-1	Aachen Univ. of Applied Science	98 Deg	630km
		Delfi-C3	Delft Univ. of Technology	98 Deg	630km
		SEEDS-2	Nihon Univ.	98 Deg	630km
		CanX-2	Univ. of Toronto Inst. for Aero. Studies	98 Deg	630km
		AAUSAT-II	Aalborg Univ.	98 Deg	630km
		Cute-1.7+APDII	Tokyo Institute of Technology	98 Deg	630km

Aug-09	Falcon 1 (Launch Failed)	NanoSail-D	NASA Marshall Space Flight Center	10 Deg	650km
		PreSat	NASA Ames Research Center	10 Deg	650km
May-09	Minotaur 1	AeroCube-3	The Aerospace Corporation	40.47 Deg	467 km
		CP6	Cal Poly, SLO	40.47 Deg	467 km
		HawkSat	Hawk institute for Space Sciences	40.47 Deg	467 km
		PharmaSat	NASA Ames Research Center	40.47 Deg	467 km
Sep-09	PSLV-C14	BeeSat	Berlin Institute of Technology	98.3 Deg	739 km
		ITUpSAT	Istanbul Technical Univ.	98.3 Deg	739 km
		SwissCube	École Polytechnique Fédérale de Lausanne	98.3 Deg	739 km
		UWE-2	Univ. of Wurzburg	98.3 Deg	739 km
Jul-09	Endeavour	Aggiesat-2	Texas A&M Univ.	51.6 Deg	347 km
		BEVO 1	Univ. of Texas at Austin	51.6 Deg	347 km

Table 1.1: Orbital parameters and launch vehicles of past CubeSats [23]

AAUSAT

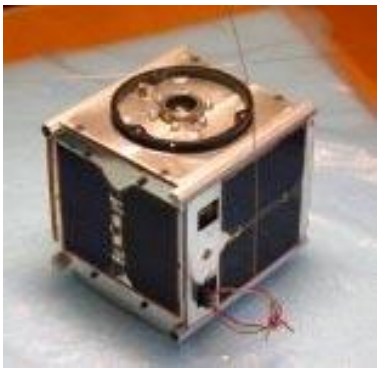

Figure 1.1: AAUSAT [2]

The AAU CubeSat was developed at Aalborg University in Denmark. First proposed in 2001 and launched in April, 2003, the AAUSAT carried a digital camera for a payload. The team's initial mission goal was to create a webpage where the public could connect to the satellite and use it to take pictures of Denmark. During the design process members of Arhus University contracted the satellite to take pictures of specific stars to measure their luminosities. The specifications for these pictures were a field of view of 100x100 kilometers and to minimal

imperfections in picture quality. To implement this more specific set of mission parameters, Aalborg University used a custom camera built and sponsored by Devitech. Devitech based their chip design on the KAC-1310, an image sensor developed by Kodak in the late 1990s. The camera chip had a resolution of 1280x1024 pixels and a 24 bit color depth. For the camera's pictures to meet the criteria set by Arhus University, an extra lens was implemented into the original camera design, and after a series of tests the team decided to use a mounted triplet lens developed by the Copenhagen Optical Company. Unfortunately, after the satellite was launched communication attempts failed, and the star imaging missions were never completed. Figure 1.2 shows a schematic of the AAUSAT camera and lens mount as was shown in the team's documentation.

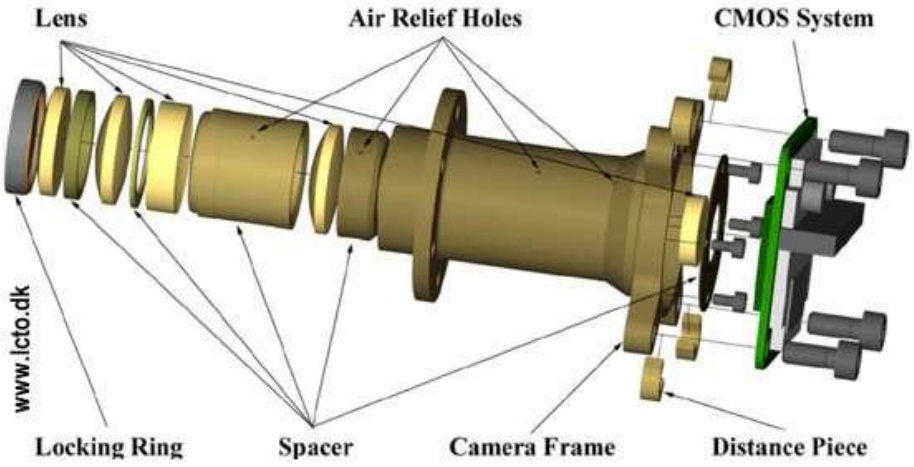

Figure 1.2: AAUSAT Camera and Lens Mount [3]

AAUSAT-II

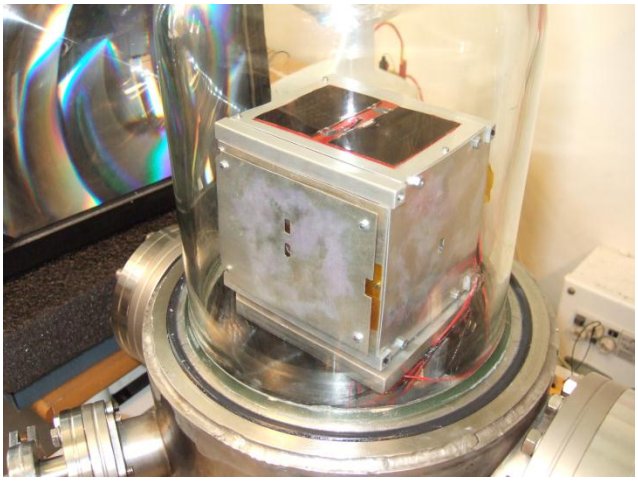

Figure 1.3: AAUSAT-II [4]

In April 2008, Aalborg University launched its second CubeSat, AAUSAT-II. AAUSAT-II contained a Gamma Ray Burst (GRB) detector provided for them by the Danish Research Institute. The goal of the mission was to study the performance and precision of the detector in space. The GRB detector measured the number of electrons hitting a 10x10 millimeter area on the outside of the AAUSAT-II. The measurements were then sent to an on-board processor that generated a data-fitted light curve (to show how many "events" the detector sensed) and the energy spectrum of the measurements (the number of "events" per energy level). Once generated, the new results were sent to the on-board computer to be transmitted to the ground station on Earth during flyover. Any interruptions or changes in the typical light curve experienced by the satellite during orbit would possibly indicate a Gamma Ray Burst in the detector's field of view. AAUSAT-II operated successfully for one year before a hardware failure occurred and the mission was terminated.

AeroCube 3

Figure 1.4: AeroCube 3 [5]

AeroCube 3 was a third generation CubeSat launched in 2009 by The Aerospace Corporation and funded by the United States Air Force Space and Missile Systems Center. Both of its predecessors, AeroCube 1 and AeroCube 2, were failed launches, so AeroCube 3 carried multiple experimental technology missions to catch up on lost experimental time. These technological experiments included the deployment of a brand new, redesigned solar power subsystem, the testing of a two-axis Sun sensor, and the testing of a new Earth sensor for navigating in future missions.

In addition, AeroCube 3 had a scientific mission, which the team divided into two phases. The first scientific phase was for the satellite to remain attached to the final stage of the launch vehicle, the Orion 38 of the TacSat-3 Minotaur, after deployment to measure the vehicle's dynamics. The CubeSat remained attached to the upper stage via a 200 foot tether, which was also attached to a reeling mechanism so that the two spacecraft could be brought together by ground command. While in this configuration, AeroCube 3 also took pictures of the Orion 38 using an on-board VGA camera and transmitted them to ground operations.

The second phase of the scientific mission occurred after the first phase had been fully carried out. After completion, the tether disengaged and the CubeSat became a free-flying satellite in LEO. The team outfitted AeroCube 3 with an eight panel, 2 foot diameter balloon that could be inflated and used as a de-orbiting device after the satellite disengaged. It was determined by the team that once the balloon deployed, the lifetime of the satellite was reduced from 1-3 years to 2-3 months. The VGA camera that had been used to take pictures of the Orion 38 was then used to photograph the level of inflation of the balloon before the mission ended.

CanX-1 (Canadian Advanced Nanospace Experiment)

Figure 1.5: CanX-1 [6]

The Canadian Advanced Nanospace Experiment CubeSat, commonly referred to as CanX-1, was launched in June 2003 by the University of Toronto Institute for Aerospace Studies. The primary mission of CanX-1 was to run multiple technological missions to test various components for use in future satellites and CubeSats. The components tested included a Global Positioning System (GPS), a magnetic based attitude control system, and a new on-board processor. The tested GPS was a commercial-off-the-shelf (COTS) Superstar GPS OEM board from CMC Electronics connected to two omni-directional antennas. The tested processor was an ARM7 central processing unit (CPU). To test the CPU the team built a custom on-board computer to house the CPU and send performance data to the ground station during flyover.

Similarly, the three axis magnetometer used was also a COTS product, a Honeywell HMR2300 three-axis digital magnetometer. The magnetometer was used in conjunction with a custom built, three coil, three-axis magnetorquer system to make a completely magnetic attitude determinations and control system (ADCS). The coils were made of AWG 32 gage magnet wire turned 380 times around a 75x55x3 mm mount.

The additional scientific missions of Can-X 1 were to test the use of CMOS imagers in space for scientific purposes, to take pictures of the Moon and Earth, and to test the use of star field pictures for attitude tracking. The satellite launched with two cameras on board. The first, an HDCS-2020 color imaging camera chip with a wide field of view lens system, was used to take the photographs of Earth. The second, an ADCS-2120 monochrome imager chip with a narrow FOV lens system, was used to take the photographs of the stars and the Moon.

CanX-2 (Canadian Advanced Nanospace Experiment 2)

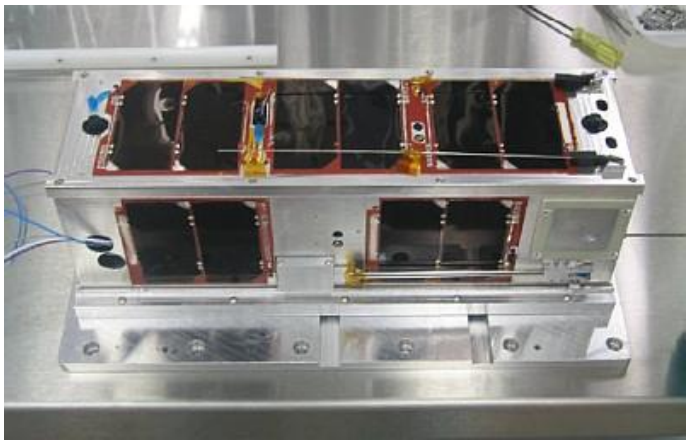

Figure 1.6: CanX-2 [7]

The successor to CanX-1, CanX-2 launched in April 2008. Like CanX-1, CanX-2 ran multiple scientific and technological experiments. The four experiments used an infrared imager, a Nano-propulsion system, an experimental GPS and a materials test for space applications. For

the infrared imaging experiment CanX-2 flew the Argus 1000 IR spectrometer to measure the amount of particles of certain infrared wavelengths and compare the spectrum to the known infrared emission spectrum of the Earth. Discrepancies in the absorption lines indicated a buildup of a certain greenhouse gas, depending on the absorption line that was detected to be distorted. The infrared experiment was sponsored by the makers of the spectrometer, Thoth. For the space materials test, CanX-2 flew onboard samples of various materials and exposed them (unprotected) to the environment of space to quantify their performance for space applications. CanX-2 also flew an onboard GPS that was used in an atmospheric occultation experiment to determine the vertical profiles of water vapor and electrons in the atmosphere. Lastly, CanX-2 also flew a prototype Nano-propulsion system to test the possibility of maintaining future satellites in formation flight. A schematic of CanX-2 with the instrument locations indicated is shown in Figure 1.7.

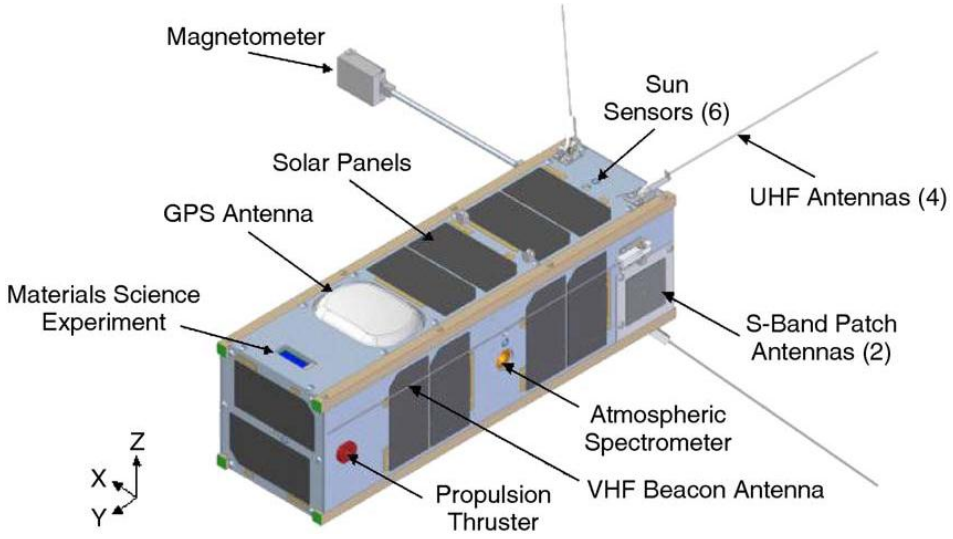

Figure 1.7: CanX-2 Schematic [8]

Compass-1

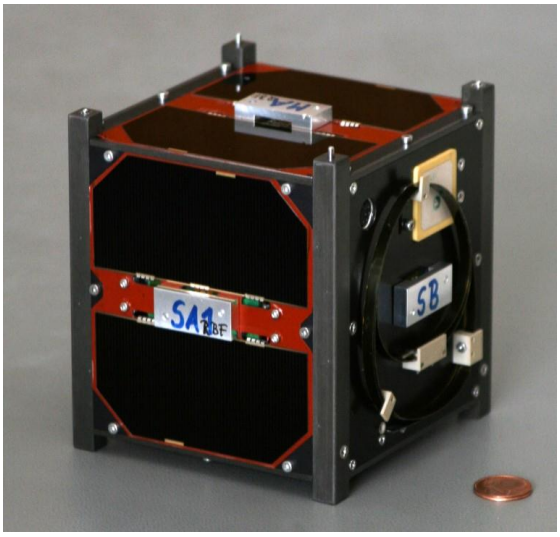

Figure 1.8: Compass-1 [9]

In April 2008, Aachen University of Applied Sciences in Germany launched its first CubeSat, Compass-1. Compass-1, like AAUSAT, carried an imaging payload used to provide 380x450 km images of the Earth from a nadir position. The chip the team integrated into the CubeSat was a commercial-off-the-shelf OV7648 CMOS camera module.

CP6 (Cal-Poly 6)

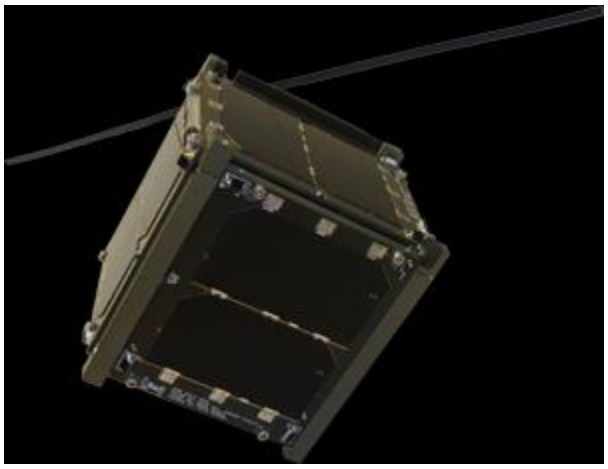

Figure 1.9: CP6 [10]

CP6, launched by California Polytechnic State University, was designed to experiment with the possibility of electrodynamically-based propulsion systems for CubeSat use. An electrodynamic propulsion system utilizes the collection of electrons in the plasma of a Low Earth Orbit (LEO) as its propellant. To determine whether such a propulsion system may be feasible CP6 was launched with an electron emitter mounted on the end of a deployable 1.8 meter boom and an electron collector mounted on a 1.1 meter boom. The collector traveled behind the emitter, which emitted a known number of electrons, to collect as many of the released electrons as possible. The team measured the efficiency of the electron collector to try and judge the effectiveness of such a collector for use in the electrodynamic propulsion system. The mission ran successfully for about 6 months.

Cute 1.7 + APD, Cute 1.7 + APD II

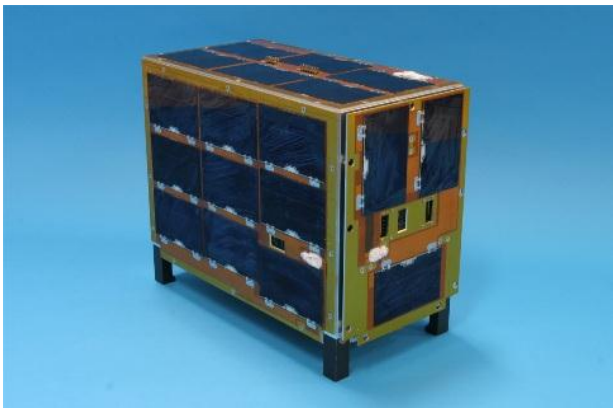

Figure 1.10: Cute-1.7 + ADP II [11]

In the past ten years, the Tokyo Institute of Technology launched three similar CubeSats: Cute 1, launched in June 2003; Cute 1.7 + APD, launched in February 2006; and Cute 1.7 + APD II, launched in April 2008. Cute 1.7 + APD II was the successor mission to Cute 1.7 + APD, and was described as being similar in structure (excluding upgrades to electronic components) to its predecessor. The primary design goal of Cute 1.7 + APD was to build a low

cost satellite out of mostly COTS products. To do this the satellite demonstrated that the OBC could be replaced by a standard commercial grade Personal Data Assistant (PDA). The PDA used was a Hitachi PDA NPD-20JWL operating on Windows CE.NET 4.1. Along with the OBC, the magnetometer, the gyro sensor, the sun sensor and the Earth sensor were all COTS parts. They were a HMR2300 by Honeywell, a combination of three ADXRS gyroscopes, a photodiode array by Hamamatsu Photonics, and a FlyCAM-CF by Animation Technology with a fisheye lens, respectively.

The scientific missions completed were the demonstration of an Avalanche Photo Diode (APD) and a de-orbiting device. The APD sensor was developed by Tokyo Tech Astronomy Laboratory to monitor charged particles with a charge under 30 keV. The de-orbit device was a 100 meter electrodynamic tether with a carbon nanotube electron emitter at the end. A current of 0.2mA would flow through the tether and be emitted into space from the carbon nanotube emitter. For the de-orbiting system to work the tether was required to be pointed perpendicular to the Earth's magnetic field.

Delfi-C3

Figure 1.11: Delfi-C3 [12]

The Delft University of Technology in Holland launched their first CubeSat, Delfi-C3, in April 2008. Delfi-C3 ran three experiments while in orbit. The first experiment was a test of the performance of thin film solar cells in the space environment. The solar cells were provided by Dutch Space and were tiles composed of 25 micrometer thick photovoltaic cells. During flight operations, the team performed a temperature test and an IV-curse test on the solar cells to gauge their space performance. The IV-curves were measured by a current sink that was programmable, and the temperature was measured through electrical resistance measurements. The second experiment was the test of an autonomous wireless sun sensor. The sun sensor was connected to its own solar cell for power and transmitted all of its data wirelessly to the on-board computer (OBC). The mission also demonstrated the use of a high efficiency transceiver for applications in Pico- and Nanosatellites, formation flights, and communications between satellites.

GeneSat-1

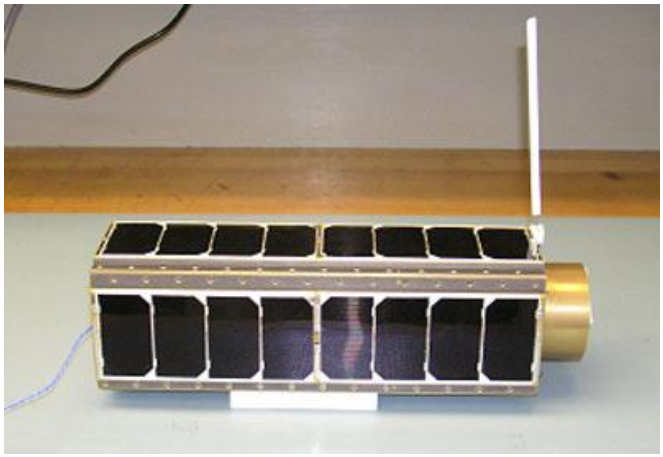

Figure 1.12: GeneSat-1 [13]

Launched in December 2006, GeneSat-1 was designed by the NASA Ames Research Center to experiment on a bacteria sample, becoming the first CubeSat to carry a biological

specimen. A growing concern for NASA is how the space environment affects the human body with prolonged exposure. To gain more insight NASA launched GeneSat-1 carrying a miniature laboratory housing various types of bacteria. They then monitored the affects that the radiation in space had on the bacteria. Not much information beyond these basic mission objectives was published for the public to view. An image of the internal laboratory can be seen in Figure 1.13.

Figure 1.13: GeneSat-1 Payload Housing [14]

HawkSat

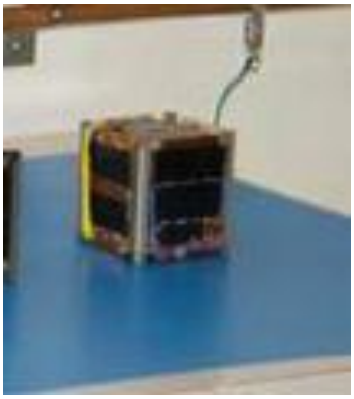

Figure 1.14: HawkSat [15]

HawkSat, developed by the Hawk Institute for Space Sciences with the University of Maryland Eastern Shore, was designed as a prototype CubeSat for the company which would be the foundation of later CubeSat designs. As a result, it was very bare-boned and carried a very limited scientific payload with little documentation. The small payload consisted of samples of newly developed aerospace materials, and the satellite collected data on the impacts of the particles in the LEO environment on the exposed materials.

ION (Illinois Observing Nanosatellite)

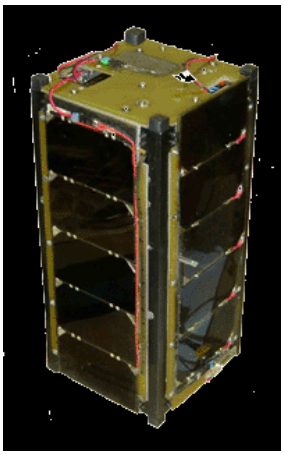

Figure 1.15: ION [16]

The University of Illinois at Urbana-Champaign (UIUC) launched its first CubeSat, the Illinois Observing Nanosatellite (ION), in June 2006 with the intention of performing multiple scientific experiments; however, no experiments could be carried out due to a launch vehicle failure. The first proposed experiment was to image and measure the Oxygen airglow from the Earth's mesosphere for the purpose of studying atmospheric dynamics. The second experiment was a demonstration of a CMOS camera intended to image the Earth. The third experiment was the demonstration of a new COTS SID processor. The final experiment was a test of a MicroVacuum Arc Thruster. The thruster was designed to be used as a part of a propulsion

system for future microsatellites, and ION intended to perform the first flight test of such a propulsion system.

MAST (Multi-Application Survivable Tether)

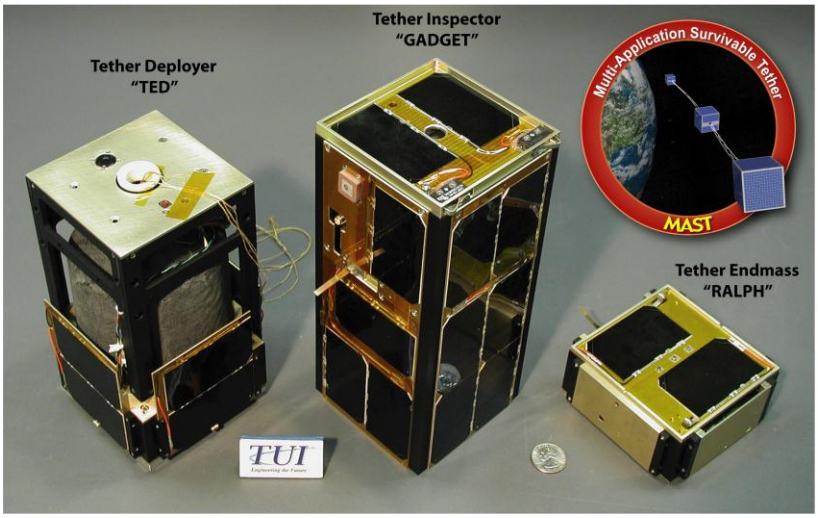

Figure 1.16: MAST [17]

The MAST CubeSats, developed by Tethers Unlimited, Inc. and Stanford University's Space Systems Development Laboratory, all launched in April 2007. The MAST experiment consisted of three CubeSats connected by a 1000 meter tether. The full experiment was carried out in three phases. The first phase occurred after the deployment of the three CubeSats from the launch vehicle and ran continuously for about three months. The experiment was an observation of tether degradation over time due to the space environment. To observe the degradation the center CubeSat utilized two sets of pincher rollers to crawl along the tether between the two end CubeSats and take pictures of the state of the tether. These pictures were then relayed to a ground station during fly-over for analysis. The fully deployed configuration of the MAST CubeSats is shown in Figure 1.17.

. At the end of the first experimental phase, one of the end CubeSats activated its 25 mN thrusters for 100s to send the CubeSat formation into rotation. The propelling CubeSat recorded

the dynamics of the system and transmitted them back to Earth. The system's rotational dynamics data was collected over 3 months for maximum accuracy and completeness.

The third experimental final phase was a demonstration of momentum exchange between CubeSats. When the propelling CubeSat was at the top of its self-induced swing it released the tether sending it into a higher orbit for continued data recording. The remaining two CubeSats were propelled into a deorbiting path.

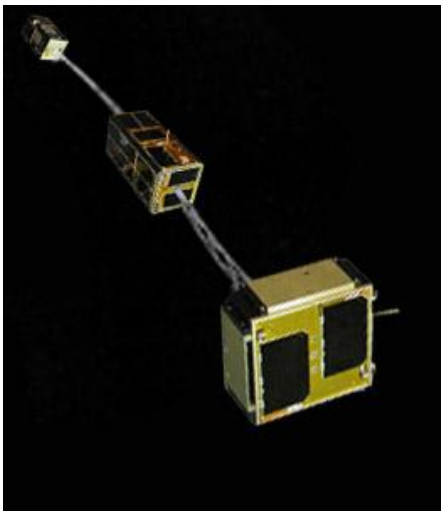

Figure 1.17: MAST CubeSats Fully Deployed [18]

NCUBE-1, NCUBE-2

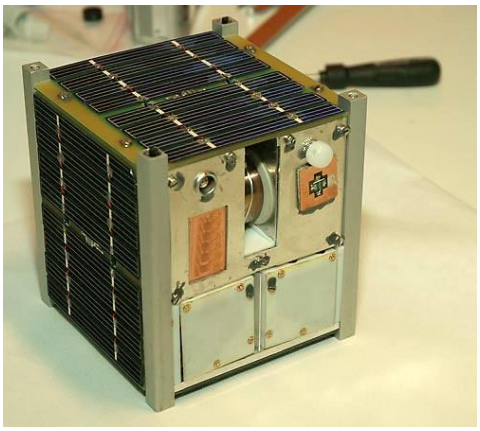

Figure 1.18: NCUBE-2 [19]

NCUBE-1, designed by the Norwegian University of Technology and Science, Narvik University College, and the Agricultural University of Norway, was scheduled to launch in June 2006; the launch vehicle failed and the satellite was lost. Though NCUBE-1 was thought of in part as simply a way to increase interest in aerospace studies in the participating universities, it also had a well-defined scientific mission. NCUBE-1 had an Automated Identification System (AIS) receiver installed on the satellite to allow tracking of large ships in Norwegian waters. The team wanted to test the ability of such a CubeSat to track all of the ships from space. To further test the functionality of the receiver, the team designed a collar to be fitted on a reindeer for additional experimental tracking data. NCUBE-2, the successor to the failed NCUBE-1, had the same structure and design as NCUBE-1, except that it also has an unspecified camera payload onboard for Earth imaging.

PharmaSat

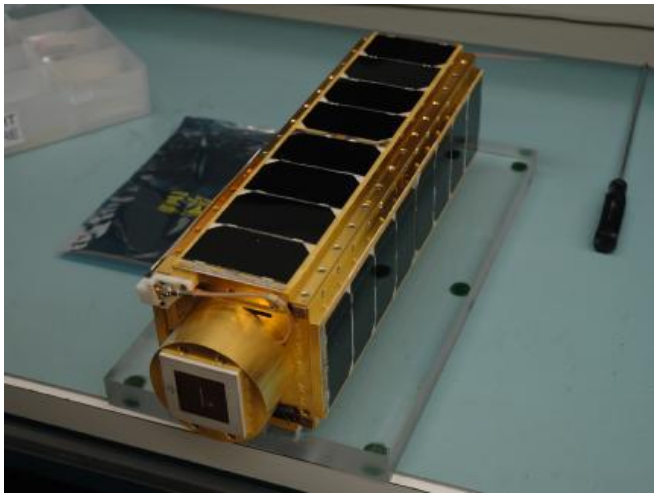

Figure 1.19: PharmaSat [20]

PharmaSat, a CubeSat developed by NASA, launched in May 2009. PharmaSat contained 48 samples of yeast that were incubated and then exposed to various antifungal chemicals. The reaction of the yeast samples to the different antifungal agents were recorded and analyzed to determine how virulent similar organisms could be in space. NASA hoped to use any results obtained from PharmaSat to further research into protecting astronauts from disease during flight operations when they are not able to receive medical treatment on Earth. No results or findings from the PharmaSat mission have been released.

QuakeSat

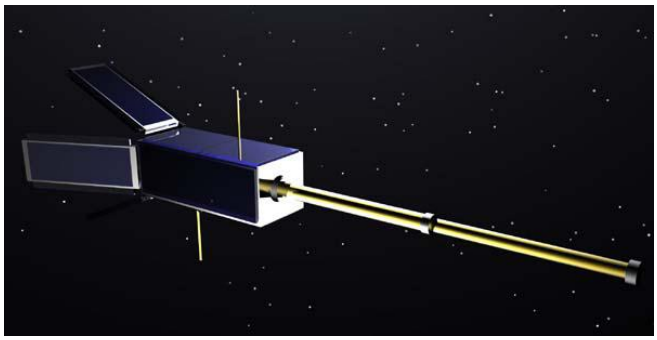

Figure 1.20: QuakeSat [21]

QuakeSat, a CubeSat jointly created by Stanford University and Quakefinder LLC, launched in June 2003. QuakeSat's mission was to use a CubeSat made of primarily COTS parts to detect traces of Extremely Low Frequency (ELF) magnetic waves emitted from Earth in LEO. Pre-existing satellites have sometimes registered disturbances in the expected values of Earth's magnetic field during or just after large earthquakes occur on the surface of the planet. The QuakeSat team hoped to be able to develop a low-cost means of detecting ELF wave propagation in the magnetic field in LEO and possibly identify the signature of a large earthquake even before it occurs. The QuakeSat ELF detection payload consisted of a single axis induction magnetometer specially calibrated to measure small magnetic disturbances. The magnetometer was then placed on a 70.1 cm boom and extended from the satellite to shield the magnetometer from electrical or magnetic interference caused by the spacecraft's electronic components. QuakeSat was designed to fly for one year, but the mission ended up lasting for two years.

SwissCube

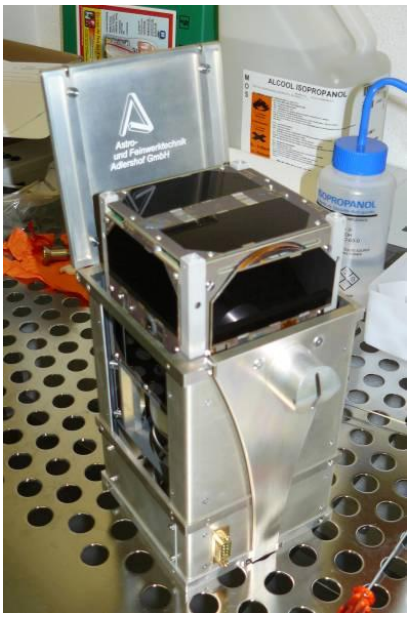

Figure 1.21: SwissCube (Encased in Deploying Mechanism) [22]

SwissCube, designed and built at the École Polytechnique Fédérale de Lausanne in Switzerland and launched in November 2009, is one of the most well-documented CubeSats to date. The SwissCube team posted a variety of design and review documents on their website, including full examinations into many different subsystems. SwissCube's primary scientific objective was to observe airglow phenomena in specific atmospheric areas over the duration of the mission. The camera selected for the mission was a COTS telescopic camera with a CMOS detector resolution of 188x120 pixels. A schematic of the camera is show in Figure 2.22. The COTS camera was selected to test the feasibility of a standardized, fairly low cost emission detecting satellite in lieu of more expensive and specifically designed satellites. Though the expected mission life was only about four months, SwissCube was still operational as of a June 2010 team website site update.

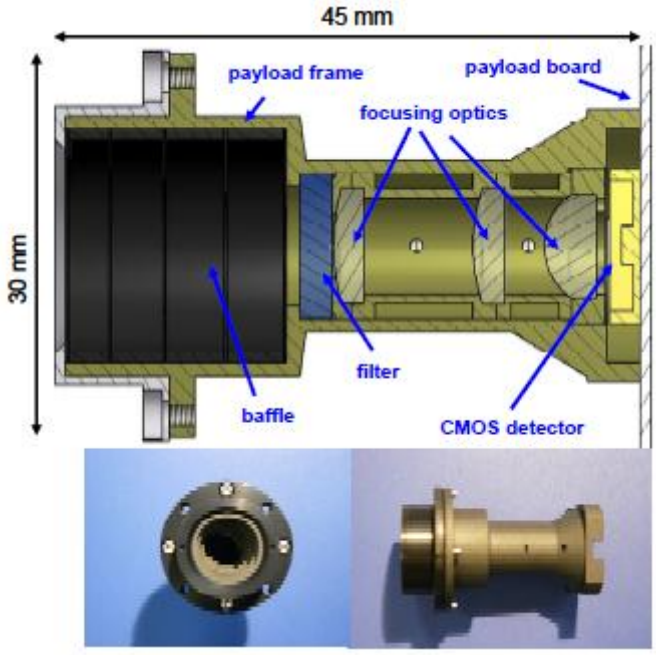

Figure 1.22: SwissCube Payload Camera [22]

1.2.2: Thermal and Environmental Literature Review

AAUSAT

The AAU team posted many documents relating to the design and analysis of their CubeSat, including dedicated pages for many different mechanical and electrical subsystems. However, there are no documents dedicated to preliminary thermal analysis on their website, and thermal analysis was not mentioned in the team's final publication. The team did mention temperature considerations in their OBC Design report, noting that the approximate range of temperature between shaded and illuminated space flight is -40°C to 80°C. The team assumed that the heat generated by the computing components themselves would be sufficient to protect the satellite's insides from extreme temperature fluctuations during orbit, and settled on selecting components meeting the industrial survival temperature standards of -40°C to 85°C. In addition,

the AAUSAT passed all thermal and functional testing from -10°C to 85°C in a thermal vacuum chamber, indicating that no issues should be expected in the field over that range of operating temperatures.

The team did not post any analytical or computational analysis for radiation effects on the CubeSat; they did however lost degradation of electronic components, bit flip errors and latchup short circuits as possible effects of radiation damage. As a result, radiation-resistant components were considered for the flight design, but ultimately were not used due to budget constraints. To compensate for possible bit flip errors, code correction techniques were used in the electronics, and a protective layer of sheet metal was applied to the spacecraft's outer panels for shielding purposes. There was no spacecraft charging analysis present in the team's documentation; although possible charging due to magnetic storms was acknowledged, no LEO charging was considered in design or analysis. Due to the spacecraft's lack of a propulsion system only onboard metals and electronic components would produce disturbances in magnetic field. The team categorized 'hard' and 'soft' iron interference effects, but stated that the levels of the interference would be determined experimentally and then calibrated out of magnetometer readings during flight operations. No final results from these experiments were reported.

AAUSAT-II

The AAUSAT-II team compiled a fairly comprehensive collection of documentation to their team websites. In a 2004 payload subsystem review, the authors mentioned that robust components are required for spacecraft design as the temperature variations can be great within a small spacecraft. The payload team stated that the AAUSAT-II committee decided that the components in their subsystem were required to survive and function within a -45°C to 85°C temperature range; however, they did not identify the source of or justification for this range.

They also state that temperature testing should be done for electronic components, but do not provide results as the tests were performed after the publish date of the paper. In an online mechanical subsystems update, the AAUSAT-II team claimed that simulations of the internal satellite temperature gave a range of -10°C to 50°C.

No analytical or computational analysis of radiation effects was documented by the team. Effects of radiation on the satellite's components were only alluded to in a small environmental section of the documentation. It is assumed that AAUSAT-II used the same radiation protection solutions as its predecessor, namely using code correction algorithms and surface protection due to the cost of radiation resistant parts. There was no spacecraft charging analysis or electromagnetic interference analysis present in the documentation; it is assumed to have used the same analysis as the AAUSAT.

CanX-1 (Canadian Advanced Nanospace Experiment)

In a 2002 progress report, the CanX-1 team stated that to conserve volume and power for other subsystems, passive thermal controls such as thermal coatings and insulations were preferred. The team also gave a summary of the expected operating temperature ranges for components on CanX-1, with the general range being about -40°C to 85°C. The limiting operating temperature range was that of the batteries during charging, with an allowable range of 0°C to 40°C. The team performed a thermal analysis simulation using the CAD software package I-DEAS, and found that using realistic surface coating properties, the temperatures ranged from a maximum of 45°C to a minimum of -27°C; however, they never state the properties of the assumed surface coatings or the final selection of surface materials.

The team considered the issue of radiation exposure and its effects on the electronics of the CubeSat. To counteract these problems, radiation-resistant components were purchased and

implemented into the final design. However, the on-board computer's processor was not explicitly resistant to radiation; it was chosen based on its history as a reliable option in LEO for the period of time considered for the mission. Error detection and correction (EDAC) code correction software algorithms were also implemented to counteract radiation damage. There was no analysis of spacecraft charging or electromagnetic interference in the team's documentation.

CanX-2 (Canadian Advanced Nanospace Experiment 2)

CanX-2's pre-launch publications made very little mention of the team's methods for predicting and analyzing the thermal environment to be experienced by their satellite. In a 2005 publication, the authors stated that temperatures from -20°C to 40°C were considered as the worst-case scenario for the CanX-2 CubeSat's NANOsatellite Propulsion System (NANOPS). In a 2006 publication, the authors stated that spacecraft materials and component placement were chosen based on a computer simulation in order to enable the use of a passive thermal control system that was reliable over a wide range of possible altitudes and orbit trajectories. However, the authors did not state which computer modeling programs were used to arrive at these critical selections.

The CanX-2 team's documentation lacks any mention of radiation effects, spacecraft charging, or electromagnetic interference. It is assumed that the team used the same techniques as mentioned in the documentation of their predecessor, CanX-1.

Compass-1

A member of the Compass-1 team performed an in-depth examination of the thermal control system requirements, finding that different configurations of solar panels and external

paneling coated in black paint gave internal temperatures ranging anywhere from -43°C to 53°C under transient conditions. Additionally, the expected internal temperature range using a configuration of multi-layer insulation and solar panels was slightly lower, from about -77°C to 31°C. 10 The operating temperatures ranges given by the Compass-1 team vary from component to component, but the limiting case belonged to the CubeSat's battery, which had an operating range of 5°C to 20°C. As a result, in addition to passively controlling the temperature using externally applied paint, the team decided to use a partially active thermal control system by attaching a heater to the battery. The team designed a closed-loop controller that used temperature readings around the battery pack to determine if the battery heater should be activated. Whenever the temperature sensors detected the temperature to be lower than 5°C, the heater was activated and remained on until the temperature of the battery reached 20°C, ensuring that the battery would be within its operating temperature at all times. However, the post-flight documents reveal that the Compass-1 team experienced issues with their active thermal control system during flight operations. Soon after deployment, Compass-1 began experiencing problems with power budgeting due to a heater malfunction. The heaters were constantly running during flight as they attempted to keep the temperature within the battery box above 5°C, draining the power from the batteries that was expected to be available for the other subsystems. After several attempts to patch the heater's code, the team disabled the use of the heater entirely, finding that the battery still functioned well enough over the entirely of the orbit period. In their flight results paper, the team stated that the active thermal control system was found to be unnecessary.

The team designed the data bus so that if a single bit of data was flipped during transfer as a result of radiation interaction, the hardware interpreted the new signal as an invalid

command. This way the operation and performance of the CubeSat's on-board computer was protected against radiation-induced damage and errors. However, there was no dedicated protector against incident radiation damage to the components themselves. Additionally, the team noted that if two bits were flipped instead of just one, a valid command may be created, leading to false readings or false commands in the OBC. No analysis of spacecraft charging or electromagnetic interference was present in the documentation.

Cute 1.7 + APD, Cute 1.7 + APD II

The Cute 1.7 + APD website specifies three areas in which their efforts to upgrade and improve subsystem components and performance over those of Cute 1 were focused; however, the thermal and environmental subsystem is not explicitly listed. In their report on the development of Cute 1.7 + APD, the team made no mention of the thermal control system selection process, but they did mention in a summary table that the CubeSat had passive thermal control. The Cute 1.7 + APD II team mentioned thermal testing in their own development report, noting that the thermostatic chamber test results indicated that the satellite would function normally in the range of -20°C to 60°C. However, there was no indication of whether or not these operating temperatures were expected during flight.

The commercial grade PDA used as the spacecraft's main onboard computer was not radiation tested. As a result, the Tokyo Institute of Technology developed and tested its own in-house radiation protected circuitry for use in the PDA. There is no mention in the documentation of the team's measures to simulate or combat spacecraft charging effects or electromagnetic interference.

Delfi-C3

Though the Delfi-C3 team still maintains a website with mission status updates, they have not posted much information on the thermal control subsystem information page. The team did mention that the thermal control subsystem was designed to be completely passive to conserve the limited mass and power budgets of the CubeSat. The team also mentioned that thermal tapes were chosen as coatings for the outside of the satellite because of their ease of application and the unlikeliness of possibly damaging the outside panels. The team made no mention of their expected temperature ranges in flight or of any simulations or testing performed before launch. No analysis of radiation effects, spacecraft charging, or electromagnetic interference was present in the team's documentation.

ION (Illinois Observing Nanosatellite)

UIUC still maintains the ION team website where the team posted updates on all of the CubeSat subsystems. Unfortunately, it seems to have been left without updates since shortly before the expected launch of ION. The team's structures page listed the operating temperature ranges of the components to be included on ION, and stated that the aim of a thermal control subsystem was to ensure that the components did not experience temperatures above or below their operational limits for extended periods of time. The testing section of ION's team website also included the thermal-vacuum testing process, and the justification for testing both worst-case hot and worst-case cold scenarios. However, the team made no mention of testing results, or any expected temperature ranges during flight operations.

Electromagnetic interference was considered and accounted for in ION's magnetometer readings. This was done using a linear model to account for the actual reading and the noise

reading due to other components onboard. The model calibrates the magnetometer by subtracting the known value of the electromagnetic interference levels of the on-board components. The team's documentation does not make any mention of radiation effects or spacecraft charging analysis.

QuakeSat

In a pre-launch paper given at a conference on small satellites, the QuakeSat team briefly discussed their thermal control subsystem and analysis. The satellite made use of a totally passive thermal control scheme, though the report did not detail the methods used to maintain favorable thermal balance. Additionally, the report stated that the thermal analysis techniques predicted a flight temperature range of -38°C to 27°C. Since the lower limit of their component operating temperature range was higher than the lowest predicted temperature, the team indicated that they would try to reconfigure the CubeSat's components and change heat dissipation rates in an effort to increase the lowest temperature expected to be more in line with their desired range. There is no mention in the team papers of any environmental analysis.

SwissCube

SwissCube employed both active and passive thermal control schemes in accordance with their preliminary thermal analysis. The team performed thermal simulations using MATLAB and COMSOL for a variety of possible orbits. In general, their expected temperature ranges were between -50°C and 50°C, with different components experiencing different temperature ranges. The biggest reason for adopting an active thermal control scheme was the predicted temperature of the batteries during flight; every simulation predicted that the lowest battery temperature would be close to exceeding the batteries operational limiting temperature of

-20°C. The onboard computer detected when temperature readings from the battery drop below -3°C and would begin to divert battery power to a resistor attached to the battery box. The electricity running through the resistor dissipated heat back into the battery box, heating the battery until it reaches 2°C. When the temperature sensors and computer detected this stopping temperature, power to the resistor would be cut off, ensuring the battery would not overheat. The SwissCube team did not post any follow-up reports with flight temperature data or the functionality of the active thermal control system.

The largest environmental concern was the saturation of the magnetometer due to the field produced by the magnetorquers. To analyze the strength of the magnetorquer magnetic field an analytical model was used to estimate the strength of the field at various distances. The magnetometer and magnetorquer were place as far away as possible within the spacecraft to minimize interference. It concluded saying that saturation can only occur where the Earth's magnetic field is greater than 45 microTeslas along one axis and this only happens when the angle between the axis and magnetic field vector is less than 46.2°. If the reading is not saturated then the value for the magnetorquer can simply be subtracted out to get a more accurate reading to the actual magnetic field at that given position. Radiation and spacecraft charging effects on the electronic equipment were not examined or reported.

The important points of the above reviews are summarized in Table 1.2.

Mission	Thermal Control Notes	Environmental Control Notes
AAUSAT	Passive thermal control Survival temperature range of -40°C to 85°C for components Thermal vacuum chamber testing found components functional from -10°C to 85°C	Outer surface coatings for radiation protection and code correction techniques Considered EMI from other components and modified sensor readings accordingly No documented spacecraft charging analysis
AAUSAT-II	Passive thermal control Survival temperature range of -45°C to 85°C for components Simulations of internal satellite temperature gave -10°C to 50°C range in orbit	Outer surface coatings for radiation protection and code correction techniques Considered EMI from other components and modified sensor readings accordingly No documented spacecraft charging analysis
CanX-1	Passive thermal control I-DEAS temperature simulations yielded expected range of -27°C to 45°C	Used radiation-resistant components and employed code correction techniques No documented analysis of EMI or spacecraft charging
CanX-2	Passive thermal control Worst case scenario expected temperatures: -20°C to 40°C range	Used radiation-resistant components and employed code correction techniques No documented analysis of EMI or spacecraft charging
Compass-1	Passive and active thermal control Expected temperature range: -43°C to 53°C Heater disabled during flight, found to be unnecessary	Employed code correction techniques to limit radiation effects No documented analysis of EMI or spacecraft charging
Cute-1.7 + APD and Cute-1.7 + APD II	Passive thermal control Thermal testing confirmed satellite function from -20°C to 60°C	Radiation-resistant circuitry developed and tested No documented analysis of EMI or spacecraft charging
Delfi-C3	Passive thermal control Applied thermal tapes to outer panels No temperature ranges or data	No documented analysis of radiation effects, EMI or spacecraft charging
ION	No mention of thermal control measures (assumed passive) Thermal testing described but no results presented	EMI considered from components and filtered out using a linear model No radiation effects or spacecraft charging analysis

QuakeSat	Passive thermal control Predicted flight temperatures of -38°C to 27°C	No mention of environmental analysis or considerations
SwissCube	Passive and active thermal control Active control consists of battery heaters activated automatically Performed multiple temperature simulations for different orbit configurations	Code correction techniques and protective circuitry to combat radiation effects Modeled EMI from Magnetorquers and filtered it out using analytical model

Table 1.2: Summary of CubeSat Thermal and Environmental Literature Review

1.3: Objectives and Methods

The objectives of the scientific payload design process are to:

1. Select a scientific instrument that can perform space science onboard a satellite the size of a 3U CubeSat.
2. Design a scientific mission that can be fulfilled using the selected instrument and other space-qualified secondary instruments.

The methodology followed to select an instrument is described below:

1. Select an instrument that fits into the mass budget of our CubeSat (4 kg total) and has a volume that can be enclosed by our CubeSat (10cm x 10cm x 30 cm). The instrument must either have space flight heritage or be space qualified.
2. Verify that the instrument fits within the CubeSat volume with other components present, that it does not exceed the allowable mass budget, and that it can be operated on the expected power provided by the power subsystem. Determine the interfacing requirements for the instrument and communicate them to the other CubeSat subsystem design teams.

The methodology followed to design a scientific mission is described below:

1. Identify the scientific function of the selected scientific instrument in a space environment. This includes determining the objects of focus for the instrument.
2. Define the orbital elements required to perform the science on the objects of focus. Determine the period of time over which the science will take place.

The objectives of the thermal control subsystem design and analysis process are to:

1. Determine the relevant thermal environment that the CubeSat will be exposed to during flight operations and establish an allowable temperature range for flight operations.
2. Perform temperature simulations using expected flight conditions to determine if the CubeSat will maintain an allowable temperature at all times during flight. If temperatures will fall outside allowable range, make recommendations for control methods to maintain temperature range at all times.

The methodology followed to determine the CubeSat thermal environment is described below:

1. Determine all modes of heat transfer that are applicable to the CubeSat during flight operations and how to quantify them. Consider both internal and external heat sources.
2. Collect component temperature specifications from other CubeSat subsystem teams. Determine maximum and minimum allowable temperatures from the collected data.
3. Establish conditions for hot-case and cold-case temperatures during flight operations using eclipse data from the mission orbital elements.

The methodology followed to perform temperature simulations is described below:

1. Select a simulation software package that is compatible with other subsystem design team efforts.
2. Simulate the temperature of the CubeSat during both hot-case and cold-case situations.
3. If resultant temperatures fall outside of the allowable range, recommend additional thermal control methods to ensure temperatures will remain within allowable limits.

The objectives of the space environment analysis and design process are to:

1. Investigate possible negative effects of spacecraft charging during flight operations. Include both standard atmospheric condition analysis and possible magnetic storm condition analysis.
2. Identify which electronic components could contribute to electromagnetic interference with other instruments. Determine the worst-case effects and what measures can be taken to alleviate these effects.

The methodology followed to investigate spacecraft charging effects is described below:

1. Identify software options for spacecraft charging simulations. Choose a software package and learn how to perform spacecraft charging analysis simulations.
2. Identify an appropriate atmospheric environment model to obtain the expected conditions to be experienced by the CubeSat. Determine both standard conditions and magnetic storm conditions for the time period of the mission.
3. Perform spacecraft charging analysis for both atmospheric cases using the predicted conditions. Determine if the calculated levels of charging exceed allowable levels, and if so, recommend possible corrective measures to prevent damage to spacecraft.

The methodology followed to investigate electromagnetic interference and its effects is described below:

1. Collect information on electromagnetic interference produced by electronic components from other CubeSat subsystem design teams. Identify the largest contributor of electromagnetic interference from collected information.
2. Identify which, if any, electronic components will have their performance negatively affected by the electromagnetic interference.

3. Select an electromagnetic simulation software package to perform electromagnetic interference. Determine the strength of the electromagnetic interference in the volume of the CubeSat. If the artificial levels of interference will negatively impact a device's performance, determine what measures can be taken to eliminate or reduce the expected interference upon that device.

The objectives of the magnetometer selection and boom design process are to:

1. Select a magnetometer that can be used by the ADCS design team to determine the Earth's local magnetic field during flight operations.
2. Design a boom to deploy the magnetometer so that electromagnetic interference will not disrupt or distort the magnetometer readings and data.

The methodology followed to select a magnetometer is described below:

1. Identify the nominal values of the Earth's magnetic field in our CubeSat's designated orbit and ensure that the selected magnetometer can detect a magnetic field of the same magnitude or greater.
2. From the pool of magnetometers that can detect Earth's magnetic field, select a flight option magnetometer by emphasizing low mass, low power usage, high resolution, and compatibility with the ADCS design team's other components, particularly the on-board computer.

The methodology followed to design a boom for the magnetometer described below:

1. Determine the minimum length of boom needed to eliminate artificial electromagnetic interference from the magnetometer's readings.

2. Design a boom to deploy the magnetometer to the appropriate length by focusing on employing a low-power deploying mechanism and limiting large deflections by the boom during flight operations. If possible, design boom to be externally stowed to limit impact on volume budget within the CubeSat.

Chapter 2: Scientific Payload Design

2.1: Scientific Instrument Selection

During the early stages of the project, a wide variety of possible payloads were examined. These possibilities included regular photographic cameras, ultraviolet imagers, infrared imagers, and particle detectors. We ultimately selected the Argus 1000 Infrared Spectrometer (AIRS) as the payload for our CubeSat mission. The AIRS is an optical sensor used to measure the quantity of particles energized in the infrared spectrum, corresponding to a wavelength range between 900nm and 1700 nm. Utilizing a linear gallium arsenide (InGaAs) photodiode array and CMOS active-pixel readout technology, the AIRS has a field of view of 1.57 square km when deployed in LEO. Developed by Thoth Technology Inc. in Ontario, Canada, the AIRS has a mass of 230 grams and has dimensions of 4.5cm x 5.0cm x 8.0cm. Its small size makes it an ideal CubeSat payload from a mass and volume budget standpoint, and has flight heritage, having been flown aboard CanX-2 in 2008. The AIRS is shown in Figure 2.1.

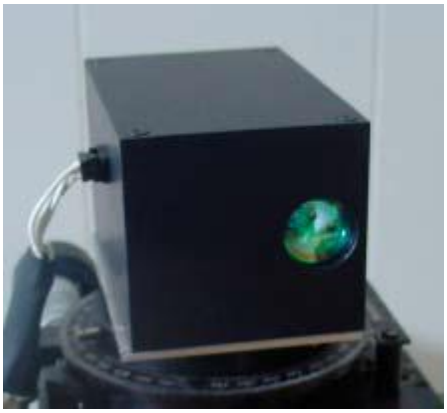

Figure 2.1: Argus 1000 IR Spectrometer [24]

The use of the AIRS has been demonstrated previously by the 2008 CanX-2 mission, so its space qualifications are reinforced by this flight heritage. While passing over Ontario, the

AIRS collected data on the number of incident particles of different energies and wavelengths. A plot of the CanX-2 collection results is shown in Figure 2.2. The recorded data was then compared to the known levels of particles in the Earthshine. The wavelengths at which the particle counts are lower than expected levels indicate that some absorption of the associated particles occurred in the atmosphere. The absorption wavelengths of common atmospheric and greenhouse gases are shown in Table 2.1. Combining this information with the data obtained with the AIRS we can calculate the amounts of these greenhouse gases in the atmosphere.

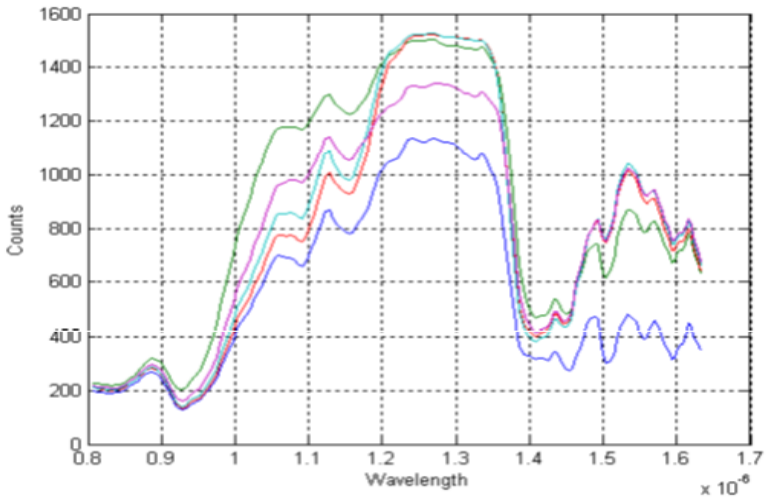

Figure 2.2: Data Acquired by CanX-2 over Ontario, Canada, December 2008 [24]

Gas	Absorption Strength
Oxygen (O_2)	1.25µm (10^{-24}mol.cm^{-2})
Carbon Dioxide (CO_2)	1.57µm (10^{-23}mol.cm^{-2}) 1.61µm (10^{-22}mol.cm^{-2}) 2.05µm (10^{-21}mol.cm^{-2})
Water (H_2O)	900nm (10^{-21}mol.cm^{-2}) 1.2µm (10^{-21}mol.cm^{-2}) 1.4µm (10^{-19}mol.cm^{-2})
Carbon Monoxide (CO)	1.63µm (10^{-22}mol.cm^{-2})
Methane (CH_4)	1.67µm (10^{-20}mol.cm^{-2}) 2.25µm (10^{-20}mol.cm^{-2})
Hydrogen Fluoride (HF)	1.265µm (10^{-19}mol.cm^{-2})

Table 2.1: Atmospheric Gas Absorption Strengths [24]

The scientific objectives of our CubeSat mission are to:

1. Obtain particle measurements pointing at nadir over the city of interest.
2. Obtain particle measurements pointing at each of the atmospheric limbs over the city of interest.
3. Use the particle measurements to determine the presence of greenhouse gases over the city of interest.

For our flight option CubeSat, we will implement the AIRS similarly to how it was implemented on CanX-2, but with expanded science objectives. The proposed sequence to generate 15 minutes of data in a 19 minute cycle is:

1. Take measurements for five minutes pointing at one of the atmospheric limbs over the city of interest.

2. Reposition the AIRS to point towards nadir to take another five minute sample over the city of interest. The repointing maneuver should take no longer than two minutes.
3. Reposition the AIRS to face the opposite atmospheric limb from the first collection period to take the last five minute sample. The repointing maneuver should take no longer than two minutes.

To further extend the amount of information collected from these samples, data recording will be taken over major United States cities over a flight operations period of one year. The resulting data will hopefully show any trends of greenhouse gas emissions throughout the four seasons in each city. Additionally, with samples being taken at various cities a more complete picture on general emission patterns can be reconstructed from our findings.

2.2: Orbital Elements

In order to fulfill these scientific objectives, an orbit for our CubeSat was proposed to fit the required ground path. Modeling and analysis of our CubeSat's orbit was done using the Satellite Tool Kit (STK), a software package developed by Analytical Graphics, Inc. (AGI). STK provides the user with a wide array of analytical tools for many aerospace and defense applications. Our team primarily used the basic orbit propagator and the STK/Space Environment and Effects Tool (STK/SEET) to model the orbit and model some of the associated environmental parameters. The proposed orbital elements are listed in Table 2.2.

Orbital Element	Value
Semimajor Axis *a*	7051 km
Eccentricity *e*	0.0
Inclination *i*	98.0°
RAAN Ω	0.0°
Argument of Latitude *u*	0.0°
Altitude	680 km
Period	98.2 min

Table 2.2: CubeSat Orbital Elements

The proposed orbit is a sun-synchronous orbit, which means that the orbital plane is fixed with respect to the Sun. This constancy of the orbit's Sun exposure over time provides the spectrometer with consistent lighting and timing of its measurements. Though orbital perturbations such as upper atmospheric drag and third body influences will have a small effect on the CubeSat's orbit, the mission life is short enough to allow these movements to be ignored. Thus, we consider that the CubeSat will be taking its measurements at the same time of day every time it flies over a certain city. An STK simulation image of the ground path of the satellite passing over the United States is shown in Figure 2.3.

Figure 2.3: CubeSat Ground Path over USA

2.3: Ground Coverage

The AIRS collection data will be downlinked to a ground station at WPI during flyover. To obtain the geolocation of the satellite at the required accuracy and at the time of the measurements, a GPS module is necessary. For our module, we selected the Trimble M-Loc MPM GPS module with matching antenna. This GPS setup has accuracy rating of better than 7 meters, a low price of $45, and has CubeSat flight heritage on the AtmoCube. The GPS module only weighs 5.7 grams and has dimensions of 25.3mm x 25.3mm x 6.9mm, making it ideal for the CubeSat mass and volume budgets. The GPS module antenna is also included, with its dimensions being 20.1mm x 20mm x 8mm. An image of the GPS module is shown in Figure 2.4.

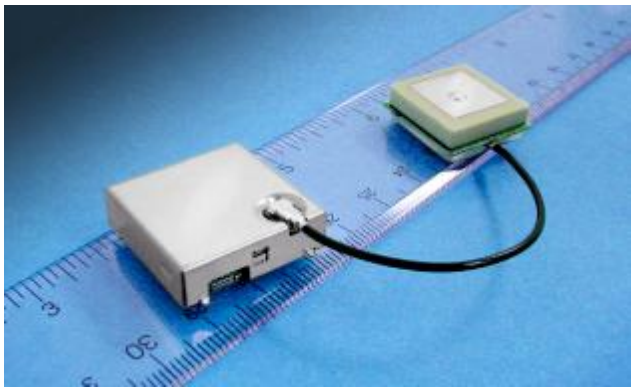

Figure 2.4: Trimble M-Loc MPM GPS Module and Antenna [41]

2.4: Data Processing and Analysis

Processing of the downloaded data is required to more accurately estimate the amounts of various greenhouse gases over each city. One method for computing spectral gas models is the use of the MATLAB code GENSPECT. This code uses the AIRS data output and the geolocation information provided by the GPS. Additionally, because clouds can absorb greenhouse gases and skew measurement results, the code includes surface cloud coverage data provided by

meteorological models. The resulting output is an accurate calculation of greenhouse gas quantities over the targeted cities.

2.5: On-Board Computer Interface

For the AIRS, the required interfacing OBC commands were simple. To begin data collection, the AIRS only requires an 'on' signal from the OBC, as the AIRS does not have multiple operating modes. Similarly, to stop data collection, the OBC command is just 'off,' as powering down the AIRS is the only way to end collection.

Connecting to the OBC is also a simple task. The AIRS outputs all of its data through a serial cable in real time. The ADCS subsystem team selected an MSP430 microcontroller which takes its inputs through serial cabling, so no conversions are required for the connection.

Lastly, we had to calculate how much data will be transmitted to the OBC and then the ground station during each fly-over. This required knowledge of how long the payload instrument will be running (previously defined as 15 minutes per fly-over) and how much data it collects in that amount of time. The resolution of the samples is also important; high quality images or measurements require more bits of storage than lower quality samples. The AIRS automatically determines the resolution of its samples by how many scans are required per sample and exposure time. For the AIRS, the number of samples can be set between 2 and 9, and the exposure time can be set between 500μs and 4096ms. We used the Equation 2.1 to calculate the quantity of data we will be collecting.

$$(exposure\ time) * (number\ of\ samples) + 100ms = time\ to\ take\ one\ sample \quad (Eq.\ 2.1)$$

Here, the 100ms is the startup time of the AIRS. Each measurement taken by the AIRS results in 532 bytes of data output to the OBC. For our mission, we want the best precision

possible in our data, so we set the exposure time to 4096ms and the number of samples per scan to 9, both maximum values. Therefore, for one city fly-over with a 15 minute data collection period, there will be 13 kilobytes of resultant data. Using STK, it was determined that we can fly over up to 4 cities, depending on launch time and eclipse time, per pass over the ground station. That means that the maximum amount of data that we will be storing and transmitting per cycle is 52 kilobytes. This number was passed along to the OBC design team, and they confirmed that amount of data is well within the limits of the technology we will be flying.

The OBC also needs to interface with the GPS. Like the payload the GPS interfaces via a serial connection. For our setup the OBC will just be continuously transmitting the location of the satellite, so no data storage is necessary. Also, one startup command is all that is necessary for the GPS to begin continuously sending its data.

2.6: Power Interface

The required standby power, nominal power, peak power, peak burst length, if it will be operating in illumination or eclipse, and any other special information. For the Argus the answers were that it didn't have a standby mode or need peak power, that it would operate in illumination only, and that the nominal voltage is 3.3 volts and the nominal amperage is 572 mA. The power group also needs to know about the operating times, the 15 minute data collection clusters. The power subsystem also needs to know the operating conditions of the GPS receiver and antenna. Once the GPS is turned on it will require a continuous 3.3 volts at 20.5 mA until the end of the mission

2.7: Structural Interface

The AIRS has specific requirements regarding its mounting to the CubeSat, as listed below.

1. There can be no obstructions between the AIRS optical lens and the target.

2. The edges of the hole that the sensor is looking out must be blackened to avoid reflections into the AIRS lens.

3. The AIRS should not be touching the spacecraft in any other locations besides the mounting surface. A 2mm gap between the AIRS and everything else is recommended by the manufacturing company.

4. The AIRS casing comes with 8 mounting screw holes on the top, of which at least six need to be used to ensure that the AIRS is secure.

5. The screws used must be 4-40 threaded and they may not penetrate the AIRS casing by more than 5mm to insure that no internal hardware is damaged. A diagram of the screw-hole placement is shown in Figure 2.5.

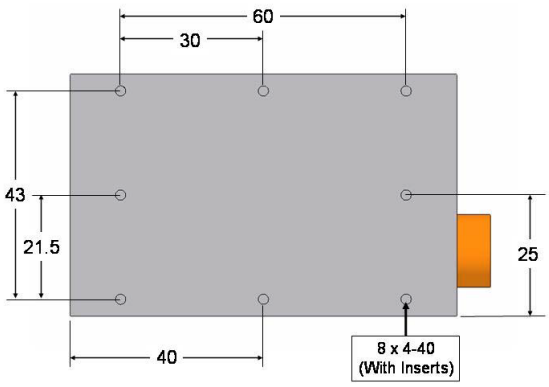

Figure 2.5: AIRS Mounting-Hole Locations [1]

6. The AIRS must not be exposed to vibrational loads lower then 10g rms, random and sinusoidal.

All of these specifications were passed along to the structures subsystem design team for consideration during design. To limit effects of disturbances on the field of view the sensor was positioned in the center of a three unit side of the CubeSat. This also allowed for room for the connectors to be connected to the sensor.

The GPS just needs to be mounted such that the antenna is not fully contained within the cube and that the receiver chip and antenna are not more than 80 mm apart from each other, because that is the length of the connecting wire. The GPS also has vibrational requirements that need to be met. These requirements are that the vibrational load cannot exceed 0.008 g^2/Hz for vibrations in the range of 5 Hz to 20 Hz, 0.05 g^2/Hz for the range of 20 Hz to 100 Hz, and -3dB/octave for 100 Hz to 900 Hz.

2.8: Thermal and Environmental Requirements

The AIRS is equipped with a radiation protective covering reducing the effects of the radiation in space. The operational temperature range of the Argus is -20 °C to 40 °C, and the survival temperature range is -25 °C to 50 °C. As for the GPS receiver and antenna, the operating temperature ranges from -40 °C to 85 °C and the survival temperature ranges from -55 °C to 105 °C.

Chapter 3: Thermal Control Subsystem Design and Analysis

Spacecraft thermal and environmental design processes are discussed in several textbooks (e.g. Wertz and Larson, 1999 [24]). Many key principles in the design process are identified in the thermal subsystem section, and all were considered during our work.

The thermal control subsystem (TCS) is designed to serve two interconnected purposes for the CubeSat; to establish and maintain a thermal balance between the spacecraft and its space environment, and to preserve the other spacecraft subsystems within their appropriate temperature ranges during flight operations. Some key terms in the discussion of a spacecraft's thermal control subsystem are defined below.

A spacecraft component's *operational temperature limits* are the maximum and minimum temperatures that a component can be exposed to while in use and still be expected to operate and perform correctly.

A spacecraft component's *survival temperature limits* are the maximum and minimum temperatures that a component can be exposed to at any time during the mission, in use or unpowered, and still be expected to operate and perform correctly when in use.

A spacecraft thermal subsystem is classified as *passive* if the desired thermal balance is maintained using surface coatings or layers of specially selected insulating material. Passive control systems are typically low cost due to a lack of complicated or complex components.

A spacecraft thermal subsystem is classified as *active* if the desired thermal balance is maintained using heaters, heat sinks, coolers, or other electric components. Active control

systems are typically more expensive than passive systems due to the additional required components.

In general, there are three separate methods of *heat transfer* by which thermal energy can be transported between bodies. *Conduction,* or *conductive heat transfer,* occurs when energy is transferred between bodies by molecular interactions. In a spacecraft, conductive heat transfer generally only occurs between components that are in direct contact. *Convection,* or *convective heat transfer,* occurs when energy is transported between bodies by a moving, heated fluid. In space environments above the atmosphere, the density of the particles in the spacecraft's immediate environment is so low that convection can be totally neglected from environmental thermal considerations. *Thermal radiation,* or *radiant heat transfer,* occurs when matter at a non-zero absolute temperature emits electromagnetic waves due to changing electron configurations within atoms. Unlike conduction and convection, radiation does not require a medium for heat transfer to occur. In space applications, radiation is the chief method of heat transfer between the spacecraft and the environment. Radiant heat transfer can also occur within the spacecraft itself if there are components that dissipate heat during operation.

Direct radiation from the Sun is a major contributor to the thermal environment of a spacecraft in orbit around the Earth. The Sun's intensity varies slightly over the orbit of the Earth due to its eccentricity; however, the average value of the sunlight's intensity over the entirety of the Earth's orbit, known as the *solar constant,* is given as $S_0 = 1367\ W/m^2$.

Indirect radiation from the Earth also plays a large role in the thermal environment of a spacecraft. Radiation reflected off of a celestial body is generally known as *albedo.* In this report, references to albedo will always refer to sunlight and radiation reflected from the Earth, unless

noted. The exact value of the Earth's albedo is dependent on the orbit of the spacecraft, but 30% is a generally accepted percentage of the solar constant reflected as albedo (this is given as about 410 W/m^2).

In addition to reflecting radiation from the Sun, the Earth also emits infrared (IR) energy as blackbody radiation. The intensity of this *Earth-emitted IR* varies depending on the temperature of the local surface emitting it and the local cloud cover preventing the surface radiation from passing through the atmosphere into space. The effective temperature of Earth-emitted IR (S_E) is generally estimated at around -18°C, and is approximately the same wavelength as IR emitted from the spacecraft. As a result, Earth-emitted IR typically cannot be reflected away from the spacecraft because the same coatings that allow the spacecraft to radiate its own IR energy away prevent the spacecraft from blocking incoming IR of similar wavelengths. A basic picture of the spacecraft's radiation environment is shown below in Figure 3.1.

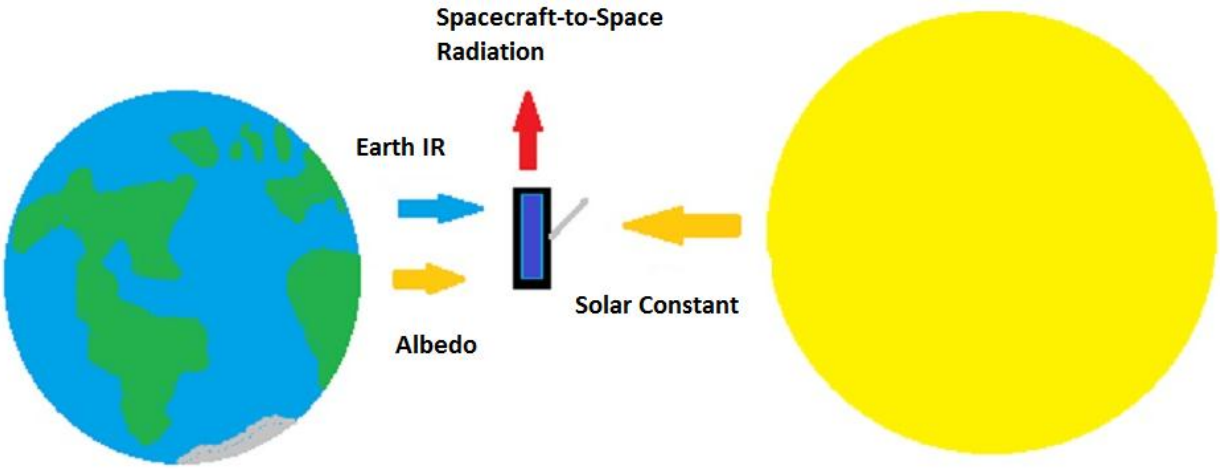

Figure 3.1: Spacecraft Thermal Radiation Environment

3.1: Determining the Allowable Temperature Range

As stated previously, the driving factor behind thermal subsystem design is keeping the satellite temperature within the temperature limits of all of the important components. The spacecraft must stay within the smallest range of survival temperatures at all times during the mission life, and must remain within the appropriate operating temperature ranges of all components being actively used at any particular time. Before performing full thermal analysis and deciding what measures might be taken to achieve an allowable temperature range, we compiled a list of all of the required temperatures for components from the other CubeSat subsystem design teams. They are summarized in Table 3.1. For components where no survival temperatures were explicitly defined, it was assumed that the survival temperature would be the same as the operating temperature; these instances are in italics.

Component	Operating Temperature Range (°C)	Survival Temperature Range (°C)
Attitude Control Thruster	-40 to 60	*-40 to 60*
Primary ΔV Thruster	**0** to 60	***0** to 60*
Gyro	-40 to 105	-65 to 150
Sun Sensor	-50 to 85	*-50 to 85*
Magnetorquer	-35 to 75	*-35 to 75*
PMAD	-10 to 40	*-10 to 40*
Solar Arrays	-25 to 140	*-25 to 140*
Magnetometer	-40 to 85	-55 to 125
Argus IR Spectrometer	-20 to **40**	-25 to **50**
GPS Module	-40 to 85	-55 to 105
Circuit Boards	-20 to 60	*-20 to 60*
On-Board Computer	-40 to 85	*-40 to 85*

Table 3.1: Operating and Survival Temperature Ranges

Additionally, the PMAD is equipped with its own active thermal control heater and radiator to ensure that the survival temperature range is maintained during the mission life, which eliminates it from possibly limiting the temperature range. As a result, the components that drove the temperature limit selection were the primary thruster and the spectrometer, with a resulting survival temperature range of 0°C to 50 °C, and a resulting operating temperature range of 0°C to 40°C.

3.2: Determining Hot and Cold Cases

A critical aspect of the CubeSat's orbit is the amount of time spent either in daylight (Sun-exposed) or shadow (eclipse). Since the Sun's radiation is the major contributor of external radiation to the satellite, the temperature of the CubeSat may vary greatly as the amount of sunlight incident upon it changes. An STK screenshot is shown in Figure 3.2; the image shows the CubeSat orbiting the Earth as seen from above, allowing the daylight-eclipse border to be clearly seen.

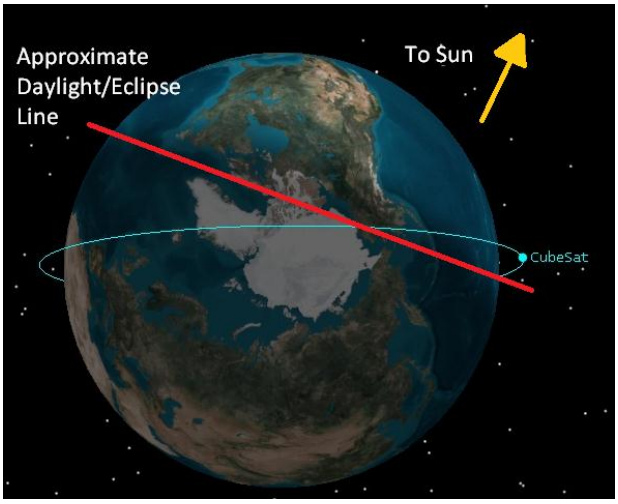

Figure 3.2: Daylight/Eclipse Border during Orbit

The time spent in eclipse during an orbit, which is crucial to determining how long the satellite will be without solar radiation to heat it, can be found using the STK orbit propagator. After finding the maximum amount of time that the satellite will spend in eclipse during its lifetime, we can calculate the coldest temperature that we expect to be experienced by the CubeSat. After running the orbit simulation, we found that the maximum time the CubeSat spent in total eclipse was about 35 minutes. Conversely, this means that the longest amount of time the CubeSat will be in direct sunlight will be the remainder of the orbit, or about 63 minutes. These findings are summarized in Table 3.2.

	Seconds	Minutes	Percentage of Period
Maximum Time in Eclipse	2098.61	34.978	35.62 %
Maximum Time in Sunlight	3793.27	63.22	64.38%

Table 3.2: Orbit Eclipse Times

3.3: Relevant Equations of Heat Transfer

There are some additional key terms in the examination of radiant heat transfer, as detailed in Incropera et al., 2007.[25] The emissive power of a body's surface per unit area can be written according to the Stefan-Boltzmann Law, Equation 3.1, below.

$$E = \varepsilon \sigma T_S^4 \quad (Eq. 3.1)$$

Here, E is the emissive power of a body per unit area, T_S is the absolute temperature of the body, σ is the Stefan-Boltzmann constant ($\sigma = 5.67 \cdot 10^{-8}$ W/m^2·K^4), and ε is the surface *emissivity* of the body. A blackbody (a perfect emitter) has an emissivity of 1.0; all other materials have emissivity values between 0 and 1.0. The Stefan-Boltzmann Law shows that the

higher emissivity of a body, the more energy it can radiate away. In general, with other factors held constant, high surface emissivity is desirable because it will allow the body to radiate more heat to maintain a desirable thermal balance if needed.

For thermal equilibrium to be achieved for our CubeSat in the space environment there must be an energy balance between the amount of radiation absorbed and the amount of radiation emitted by the spacecraft. An expression for the satellite's energy balance can be obtained by setting the incoming rate of heat flux (W/m^2) equal to the outgoing heat flux, as shown in Equation 3.2.

$$\dot{Q}_{in} = \dot{Q}_{out} \quad (Eq.\ 3.2)$$

This expression can be expanded to include terms for every method of heat transfer:

$$\dot{Q}_{Sun} + \dot{Q}_{Albedo} + \dot{Q}_{EarthIR} + \dot{Q}_{Power} = \dot{Q}_{CubeSat\ to\ Space} + \dot{Q}_{CubeSat\ to\ Earth} \quad (Eq. 3.3)$$

The terms of this equation are explained in Table 3.3.

Term	Meaning	Formula
$\dot{Q}_{Sun}$	Direct solar radiation absorbed	$\alpha A_i S_0$
$\dot{Q}_{Albedo}$	Albedo radiation absorbed	$\alpha A_i (0.3 * S_0)$
$\dot{Q}_{EarthIR}$	Earth IR radiation absorbed	$\alpha A_i S_E$
$\dot{Q}_{Power}$	Power dissipated by internal components	(experimental/specified)
$\dot{Q}_{CubeSat\ to\ Space}$	Radiation emitted to space	$\varepsilon\sigma A_i (T_{CubeSat}^4 - T_{Space}^4)$
$\dot{Q}_{CubeSat\ to\ Earth}$	Radiation emitted to Earth	$\varepsilon\sigma A_i (T_{CubeSat}^4)$

Table 3.3.: Energy Balance Equation Terms

3.4: Baseline Temperature Analysis

The baseline temperature for the CubeSat can be estimated using Equation 3.3. The energy balance for each surface of the CubeSat can be obtained using the appropriate $\dot{Q}$ terms for each side. Once all sides have been considered, the total energy balance of the six-sided body can be evaluated, resulting in a first-order approximation for the equilibrium temperature. The equation for each side is derived below. For the baseline thermal analysis, it is assumed that the Sun-facing side will always be normal to the Sun, the Earth facing side will always be normal to the Earth and opposite of the Sun side, and that the other faces will be normal to neither the Earth nor the Sun. Though these constraints are very unlikely to be constantly satisfied during orbit, they are adequate to perform the analysis. It is also assumed that the CubeSat is in daylight, as the daylight portion makes up the majority of the orbit.

The purpose of this simple baseline exercise is to give an estimate of the thermal environment to be expected during flight. Once a baseline is established, more advanced thermal analysis can be performed with software tools using the baseline as a guide for selecting parameters.

One side of our CubeSat will act as the de-facto solar array. To avoid unnecessary complications in design and make the most of our limited volume and mass budgets, our CubeSat will have the power-generating solar panels on the side of our CubeSat. The attitude and control subsystem will keep the solar array continuously pointed at the Sun during orbit to maximize the usable power for our CubeSat, and ideally the array will always be normal to the Sun and its radiation.

Obviously, to obtain the most power, the solar cells must be installed on the face of the CubeSat with the largest area. As a result, the solar panels are mounted on one of the long sides of the spacecraft, with an area of 300 cm^2 (0.03 m^2). Due to the off-the-shelf nature of our solar panels, the solar array side of the CubeSat will not be entirely covered in panels. This means that the entire surface will not have the same emissivity and absorptivity values. It is assumed that the solar array covers 85% of the side of the CubeSat (255 cm^2, or 0.0255 m^2). The other 15% of the panel (45 cm^2) will be thermally coated. The resulting equation for the emitted and absorbed radiation is shown in Equation 3.4.

$$\dot{Q}_1 = \dot{Q}_{Sun} - \dot{Q}_{CubeSat\ to\ Space}$$
$$= (0.85\alpha_{SP} + 0.15\alpha)A_1 S_0 - (0.85\varepsilon_{SP} + 0.15\varepsilon)A_1\sigma(T^4_{CubeSat} - T^4_{Space}) \quad (Eq.3.4)$$

One side of our CubeSat will be opposite of the solar panel side, and will be constantly pointed towards Earth along a normal. As a result, this side will be constantly radiating towards the Earth and absorbing both the Earth's emitted radiation and its reflected Albedo. This side will contain no solar panels or other external coverings, so we will assume that all of its area (300 cm^2) will be thermally coated. The resulting energy balance equation is shown in Equation 3.5.

$$\dot{Q}_2 = \dot{Q}_{EarthIR} + \dot{Q}_{Albedo} - \dot{Q}_{CubeSat\ to\ Earth}$$
$$= \alpha A_2 S_E + \alpha A_2(0.3 * S_0) - \varepsilon\sigma A_2(T^4_{CubeSat} - T^4_{Earth}) \quad (Eq.3.5)$$

The two long sides that will be perpendicular to the incident sides will not receive any incoming radiation from either the Sun or the Earth. As a result, the only radiant heat transfer from these sides will be radiation emitted to ambient space. These sides will be covered entirely in thermal coating (two sides of 300 cm^2 each). The resulting expression for each side is shown in Equation 3.6.

$$\dot{Q}_3 = \dot{Q}_4 = -\varepsilon\sigma A_i(T_{CubeSat}^4 - T_{Space}^4) = \varepsilon\sigma A_3\left(T_{CubeSat}^4 - T_{Space}^4\right) \qquad (Eq. 3.6)$$

Like the non-incident long sides, the only heat transfer occurring at the non-incident short sides is the radiation of heat into ambient space. These sides will also be entirely covered in thermal coating; however, because they are the ends of the CubeSat, they will be smaller than the long sides (100 cm^2 each). The resulting expression for each side is shown in Equation 3.7.

$$\dot{Q}_5 = \dot{Q}_6 = -\varepsilon\sigma A_5\left(T_{CubeSat}^4 - T_{Space}^4\right) = \varepsilon\sigma A_5\left(T_{CubeSat}^4 - T_{Space}^4\right) \qquad (Eq. 3.7)$$

Though each individual equation 3.4-3.7 may not be zero, the sum of the six radiation equations must be zero for thermal equilibrium to occur, as in Equation 3.8.

$$\dot{Q}_1 + \dot{Q}_2 + \dot{Q}_3 + \dot{Q}_4 + \dot{Q}_5 + \dot{Q}_6 = 0 \qquad (Eq. 3.8)$$

Values of the absorptivity and emissivity of both the solar panels and the surface coating are based on the assumption of silicon solar cells and black paint material. The values for the constants and variables are listed in Tables 3.4 and 3.5.

Parameter	Value
$A_1 = A_2 = A_3 = A_4$	0.0300 m^2
$A_5 = A_6$	0.100 m^2
σ	$5.67 \cdot 10^{-8}$ $W/m^2 \cdot K^4$
T_{Space}	3 K
S_0	1367 W/m^2
S_E	231 W/m^2

Table 3.4: Thermal Balance Parameters

	Absorptivity	Emissivity
Black Paint	0.97	0.85
Silicon Solar Cells	0.75	0.83

Table 3.5: CubeSat External Surface Properties

The CubeSat temperature is found to be approximately 277 K, or 4 °C. This temperature indicates that a thermal balance is achievable for our CubeSat, and that the selected black paint is a good preliminary estimate for advanced software analyses.

3.5: Temperature Simulations in SolidWorks

For more thorough thermal energy balance analysis, we used the Simulation Module in SolidWorks 2010. SolidWorks is a Computer-Aided Design (CAD) software package that allows engineers to create virtual models of both individual parts and complex assemblies of components. The CubeSat Structural, Power and Propulsion Subsystem teams all used SolidWorks extensively during their project work to model flight-option components and arrange the components inside of the CubeSat. SolidWorks also includes a fairly powerful simulation module that allows the user to perform many types of engineering analysis, including structural, thermal, vibrational, and dynamic loads. Though the thermal solver is not as powerful or versatile as a dedicated multiphysics solver like COMSOL or ANSYS, using SolidWorks for thermal analysis allows us to share models with the other design teams.

The SolidWorks thermal simulation model uses the above heat transfer equations (and other, more complex versions) to solve the complete energy balance problem. After a study is created, the user may input any required thermal parameters, including the radiation, heat flux and heat power thermal loads required for our specific analysis. For each type of thermal

loading, the user defines the associated parameters, such as emissivity, view factor, flux strength, or ambient temperature.

Using a CAD model of our CubeSat, we applied the appropriate thermal loading to the spacecraft and ran a temperature simulation. The results are presented below.

3.5.1: Hot Case (Daylight)

For the first analysis case, we simulated our CubeSat in orbit during daylight similar to the baseline analysis. The CubeSat has surface emissivity values simulating a black paint surface coating and Silicon solar cells, as in the baseline. A summary of this case is shown in Table 3.6 and a three-dimensional plot of the surface temperatures is shown in Figure 3.3. The surface temperature is from 14.7 °C on the Earth-incident side to 31.7 °C on the Sun-incident side. These temperatures are higher than the baseline analysis, but they still fall well within the required operating and survival temperatures of the CubeSat components.

The hot case simulation shows that during solar illumination, the Sun-facing side warms more than the rest of the CubeSat (as could be expected). Most of this heating will occur on the solar panels themselves, which will provide another sort of barrier between the external thermal environment and the delicate components within the satellite. The entirety of the surface of the satellite remains within the allowable limits, indicating that no extra thermal protection is required for this case. However, for extra precaution, a section of multi-layer insulation could be placed underneath the Sun-facing side external panel to ensure that excess heat on that side cannot be transferred through the CubeSat surface into the bus of the satellite.

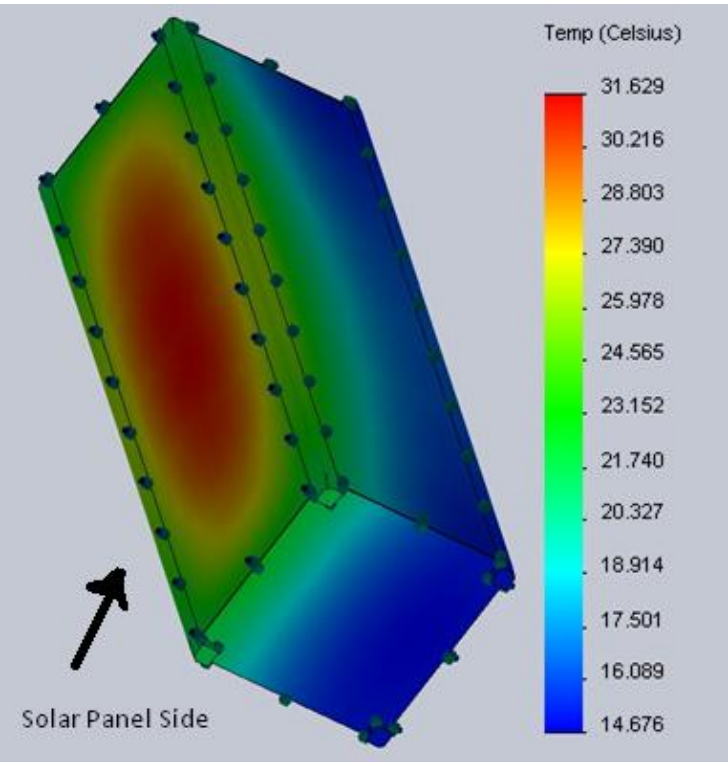

Figure 3.3: Hot Case Temperature Analysis

Daylight (Hot) Case	
Surface Emissivity	0.83 - 0.85
Simulated Solar Cell	Silicon
Simulated Coating	Black Paint
T_{Space} (K)	3
S_0(W/m^2)	1367
S_E (W/m^2)	231
Radiation to Space View Factor	1.0
Assumed Internal Heat Dissipation (W)	1.0 W
Calculated Surface Temperature Range(°C)	14.676 – 31.629
Within Temperature Range?	**YES**

Table 3.6: Hot Case Thermal Results

3.5.2: Cold Case (Eclipse)

For the second analysis case, we simulated our CubeSat in orbit during an eclipse period. Like the first simulation, the satellite has surface emissivity values simulating a black paint surface coating and Silicon solar cells. A summary of this case is shown in Table 3.7 and a three-dimensional plot of the surface temperatures is shown in Figure 3.4. The surface temperature is -12.2 °C on the Earth-incident side and -23.9°C on the solar panel side. These temperatures fall outside of the allowable temperature range set by our components. This means that actions must be taken in the thermal subsystem design to rectify this issue and maintain the satellite's operating temperatures. Note that in this case, because the solar panels are not Sun-exposed, they are not on the warmer side of the satellite.

The cold case simulations show that the CubeSat will drop below the minimum temperatures for a few of the components. When the satellite passes behind the Earth, it stops receiving solar radiation, the major source of energy absorbed by the CubeSat during thermal balancing. Luckily, the time spent in cold case conditions behind the Earth and out of the Sun's radiation is shorter than the time the CubeSat spends in daylight, and the average time spent in eclipse is only 10% of the period time (due to the movement of the Sun over the satellite's lifetime). Still, the fact that the temperatures are shown to be this low means that measures must be taken to try and bring the temperature of the satellite back to the predefined allowable limits. Because the difference between the allowable temperature and the simulated temperature is relatively small, it is likely that the difference can be made up using passive techniques.

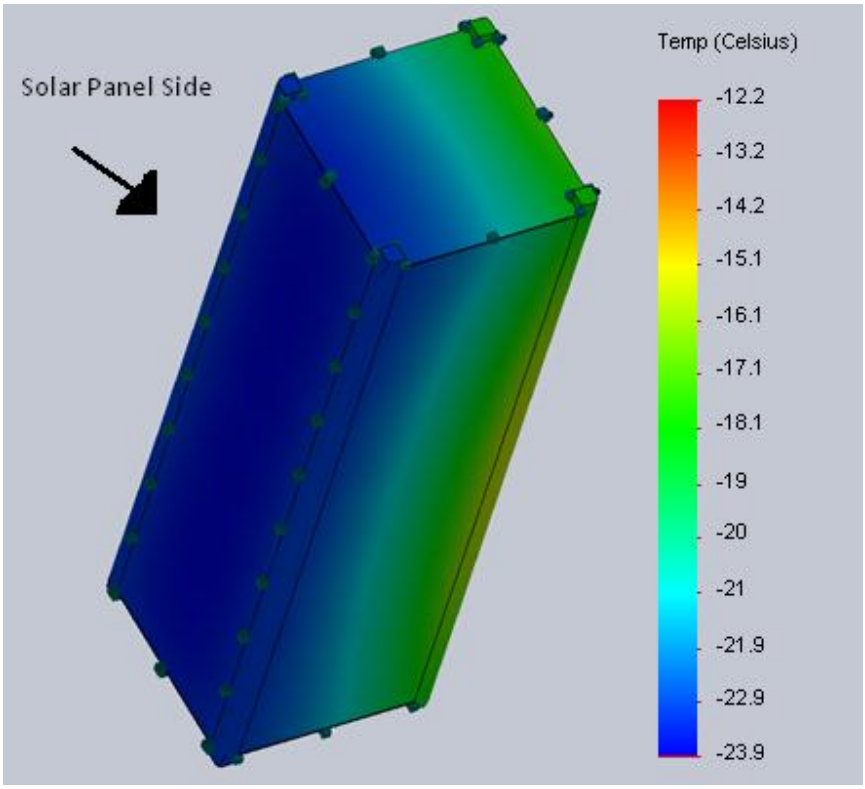

Figure 3.4: Cold Case Temperature Analysis

Eclipse (Cold) Case	
Surface Emissivity	0.83 - 0.85
Simulated Solar Cell	Silicon
Simulated Coating	Black Paint
T_{Space} (K)	3
S_0(W/m^2)	0 (Not seen during eclipse)
S_E (W/m^2)	231
Radiation to Space View Factor	1.0
Assumed Internal Heat Dissipation (W)	1.0 W
Calculated Surface Temperature Range(°C)	-12.2 – -23.9
Within Temperature Range?	**NO**

Table 3.7: Cold Case Thermal Results

3.6: Thermal Control Subsystem Conclusions

Based on the SolidWorks simulations, temperature only becomes a problem for our CubeSat during the eclipse portions of our orbit. Our simulations show that the biggest thermal issue encountered during orbit will be excess heat loss during the time when the satellite is out of the Sun's light. To keep the goal of maintaining a passive thermal control system for reduced complexity and systems requirements, the best option for reducing the amount of heat lost by the CubeSat during eclipse is to install multi-layer insulation within the CubeSat.

Multi-layer insulation (MLI) is commonly used on full-scale satellites as a method of thermal control due to its low mass, low volume, and simplicity. MLI blankets are made up of multiple thin layers of low-emittance materials with layers of relatively poor heat conductors between them. As a heat flux comes into contact with the MLI blanket, each low-emittance layer must reach thermal equilibrium within the blanket for overall thermal equilibrium to be satisfied. The result is a thin sheet of material that greatly reduces radiation losses in each layer, including nearly halving losses in each of the first few layers of MLI. However, the effectiveness of MLI drops off as more and more layers are added to the blanket. Increasing the number of layers after about 10 will not bring a large advantage to our CubeSat, and will increase the mass (albeit by a small amount), which in undesirable.

Chapter 4: Space Environmental Analysis and Design

4.1: Spacecraft Charging

Spacecraft charging is the development of an electric potential due to the accumulation of charge deposited by ambient plasma interactions with the surface of the spacecraft. Spacecraft charging is a vital part of any design and analysis of a mission in the space environment because at any altitude it can potentially be a source of failure While uniform charging is not necessarily a problem on the spacecraft due to its distribution, differential charging certainly can cause issues for the other spacecraft subsystems.. Differential charging conditions can cause electrical arcing across the differential surfaces, resulting in damage not only to the repespective surfaces but also to the sensitive instrumentation and electronics. If charging is ignored, it can cause irreparable damage to a spacecraft or its components resulting in the loss of the satellite and the ultimate compromise of its intended mission or objective. However, if charging is deemed a threat to the spacecraft with proper analysis, techniques exist to either mitigate or reduce the effects of charging and its resulting harm on the spacecraft.[36]

Many software analysis tools have been devloped to model the spacecraft charging, including NASCAP-LEO, NASCAP-GEO, SPIS, and MUSCAT. These software tools can analyze a variety of possible space environments given certain parameters of the orbit and dates of flight operations. Environmental parameters can be found using online model databases from NASA, including the International Reference Ionsphere (IRI) model.

There are two main objectives of this analysis, the first is to use parameters given from the IRI model and input them into charging analysis software in order to identify what threat, if any, spacecraft charging poses to a cubic satellite in an circular orbit at 98 degrees inclinication

and at an altitude of 673 km. The second objective is to obtain information on magnetic substorms and input the data into the analysis software to determine the level of spacecraft charging during the considered magnetic storm.

4.1.1: Spacecraft Charging Modeling

The CubeSat design in its 1 unit configuration is a 10 cm cube. Acceptable designs vary between 1, 2, and 3 unit configurations. Other restrictions include total mass requirements based on the unit size in addition but not limited to material restrictions, structural integrity, and pressurized containers. Based on these requirements and the scientific payload that we are considering it is more desirable to work with a 2 or 3 unit configuration. As a result, the spacecraft charging analysis will be performed on both of these configurations (for additional information on CubeSats and their requirements please see [26]).

As mentioned, spacecraft charging occurs due to charged particles in plasma depositing charge which translates into an electric potential on the surface of the spacecraft. We consider the spacecraft passing through a plasma consisting of electrons and ions with number densities N_e and N_i (particles/m^3), temperature T_e and T_i (K), mass m_e and m_i (kg), and charge q_e and q_i (Cb), respectively. The average thermal velocity of a particle is given by Equation 4.1.

$$v_{avg} = \sqrt{\frac{2kT}{\pi m}} \qquad (Eq. 4.1)$$

In the plasma, the thermal velocities of electrons far exceed the velocities of the positive ions because they are much less massive than the ions. Thus the electrons deposit charge faster to the spacecraft than the ions. The overall result is a non-zero flow of the electrons and ions to and

from the surface of the spacecraft. This flow creates an electric current describing flow to and from the surface; this current flux (A/m^2) is shown in Equation 4.2.

$$I_i = \frac{1}{2} q_i N_i v_{avg} \qquad (Eq. 4.2)$$

The steady state condition of the current flux will show the final charging level of the surface charging on the spacecraft. As Kieth notes [27], the overall net current flux will be zero when the steady state condition has been reached as shown in Equation 4.3.

$$I_{elec} + I_{ion} + I_{pe} + I_{sec} + I_{back} + I_{art} = 0 \qquad (Eq. 4.3)$$

Here, I_{elec} is the electron current, I_{ion} is the ion current, I_{pe} is the emission due to the photoelectric effect, I_{sec} the secondary electron current, I_{back} the back scattered electron current, and I_{art} is the artificial current. Based on further analysis the final steady state electric potential should be approximately equal to the temperature of the electron (expressed in electron volts). [2] Spacecraft charging has two possible environments that it can occur in. While the spacecraft is in the eclipse with no sunlight charging occurs primarily due to electron interactions. As the charge reaches its final values the electromagnet force starts to repel additional electrons and attract positively charged ions. While the spacecraft is in the sunlight portion of its orbit the sunlight can stimulate electron emission known as the photoelectric effect in addition to the positive ion flow to the surface. As a result the spacecraft has an overall positive charge while in the sunlight. Figure 4.1 illustrates both circumstances of the surface of a spacecraft in sunlight and in shadow. [2]

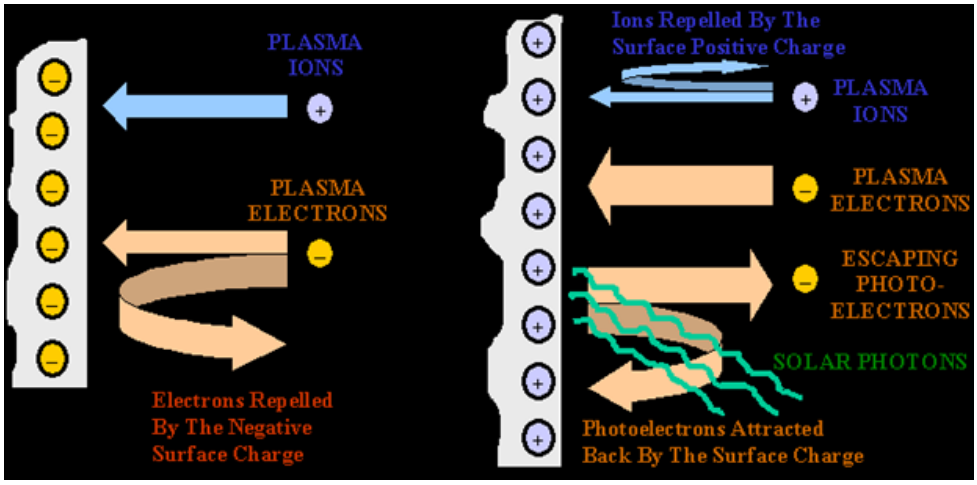

Figure 4.1: Shadow (left) and Sunlight (right) Conditions for Spacecraft Charging [27]

During sunlight exposure it is possible for the geometry of the spacecraft to cause shadows to develop on its own individual components. For instance, if a corner of a spacecraft receives sunlight at a specific angle then it is possible for that corner to create a shadow onto surfaces behind the corner. This causes a sunlight condition on some surfaces but shadow conditions on others; this differential charging is the most dangerous and most likely to cause an arc to form given sufficient voltage on the differential surfaces and cause damage to the spacecraft. Differential charging due to the spacecraft creating shadows on itself is illustrated in Figure 4.2. [2]

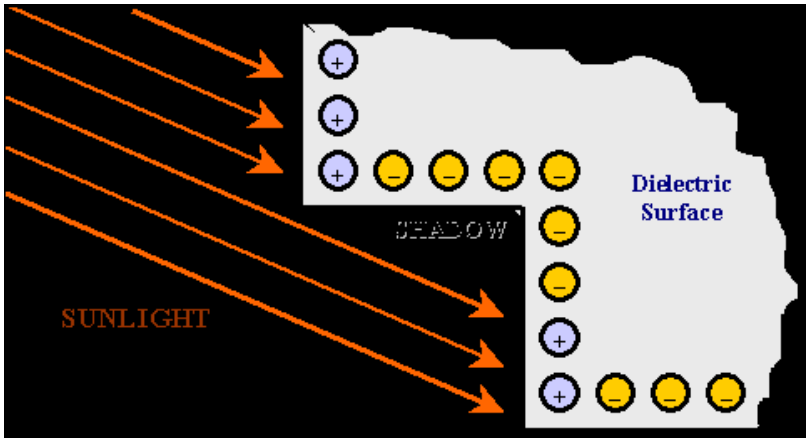

Figure 4.2: Self-Shadowing of Spacecraft Causing Differential Charging [27]

In LEO the spacecraft velocities (~ 8 km/s) required for orbit are much faster than the speed of vibration or sound through the surrounding plasma. As a result, a shockwave forms at the leading portion of the spacecraft. The spacecraft velocity is also greater than that of the thermal velocity of the positive ions (~1 km/s) but not the electrons (~200 km/s). As a result, the electrons continue to create a charge on the entire surface of the spacecraft. However, the ions are only able to deposit charge on the leading portion of the spacecraft and have a significantly reduced rate of positive charging on the trailing portion, as illustrated in Figure 4.3. Due to this phenomenon differential charging occurs which can potentially lead to arcing if the charging levels becomes large enough.

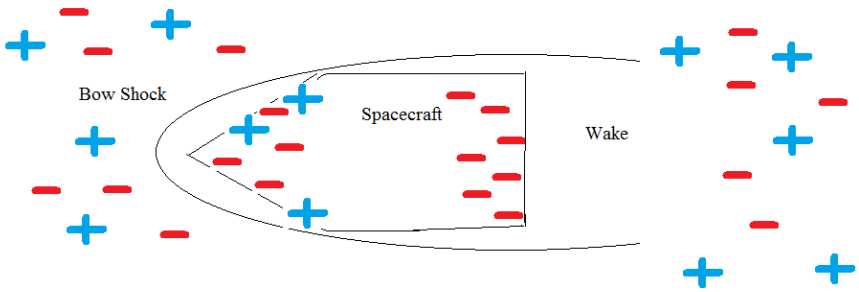

Figure 4.3: Differential Charging Due to Wake Effects

Research was done on other analysis performed on spacecraft charging in lower earth orbit. In the LEO environment, the dominating population of electrons and ions are relatively low energies. Meaning the chance of arcing onboard a spacecraft, with low operating voltages, is extremely low in the LEO orbital environment. In fact, with voltages on spacecraft below 55 V arcing has never been observed. However, voltages from 55 to 150 and beyond can arc in LEO and cause serious damage to components, especially the solar arrays which tend to accumulate high voltages and thus are most likely to arc. Charging levels that present a detrimental threat to a spacecraft and its operations exists in plasma where energy levels are roughly 10 to 25 keV

dominate the surrounding environment. At low altitudes charging levels are held below levels where arcing would occur. Based on the Power team subsystem the possible voltages are much lower than the 55 volts threshold, the power subsystems projection for our system is between 3.3 and 5 volts. Preliminary analysis based on these studies suggests that spacecraft charging on the CubeSat should be low enough where it is not an issue.[30], [31]

Given certain conditions the sun sporadically releases large quantities of particles from its surface and launches them toward the planets at extremely high speeds. Occasionally, the sun will fire these super energetic particles toward the Earth. These particles interact with the Earth's magnetosphere and some penetrate through the atmosphere. The interactions typically occur near the magnetic polar areas where the highly energetic particles interact with the atmosphere, producing the phenomena known as the aurora. To model this behavior in lower Earth Orbit the IRI model was used in the years of 2011 through 2012 and altered the Sunspot Number (Rz12) to reflect an increase in solar activity. The magnetic field lines near the cusp allow the particles ejected from the sun to get in close proximity to Earth as seen in Figure 4.4.

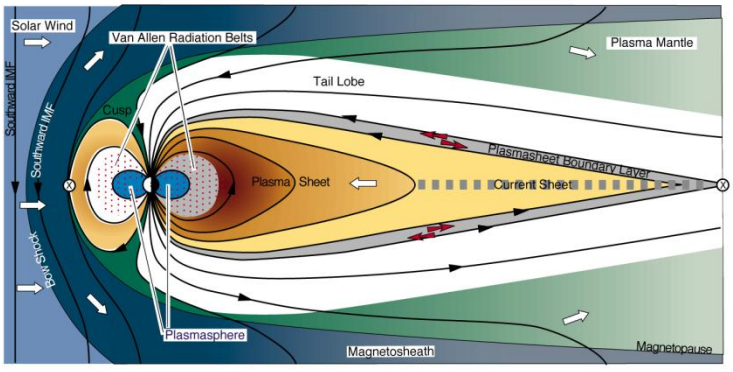

Figure 4.4: Earth's Magnetosphere [32]

4.1.2: Spacecraft Charging Software Analysis

Various numerical codes have been developed with the specific purpose of simulating spacecraft charging under different environments. For use in this analysis three software were compared in order to determine which would best suit our needs. We compared the Multi-Utility Spacecraft Charging Analysis Tool (MUSCAT), NASA Spacecraft Charging Analyzer Program (NASCAP), and the Spacecraft Plasma Interaction System (SPIS). SPIS was ultimately chosen for our purposes because it was developed by Office National d'Etudes et de Recherches Aérospatiales (French Aeronautics and Space Research Center). Also, SPIS is not subject to the International Trade in Arms Regulations (ITAR) which prohibits the use of NASCAP around non-US citizens which is not possible in a university setting. However, SPIS is not able to consider differential charging effects from the spacecraft's wake as it moves through plasma in LEO.

SPIS allows the input of 2 separate populations of electrons and of ions. It allows for the change in their associated number density, as well as the several components of the net current to the spacecraft's surface. It also enables the user to alter the capacitance of the spacecraft.

The IRI model was used in order to predict the atmospheric conditions that the CubeSat would be exposed to. These conditions would also be input into the chosen software in order to run the spacecraft charging analysis on it. Data extracted from the model would be the electron densities, electron temperatures, and ion temperatures, at an altitude of 673 km as specified in the mission requirements. These variables would range over latitudes of -90, -45, 0, 45, and 90 and day and night from 2010 until 2012 which was the maximum amount of prediction using the

model. This was done to obtain maximum and minimum temperatures and densities that the CubeSat would be exposed to over the next two years.

Extracting the minimum and maximums from the IRI model during day and night conditions at a high, middle, and low latitude shows the range of conditions the CubeSat may experience while in orbit. Table 4.1 is the electron temperature, Table 4.2 is the ion temperature, and Table 4.3 is the electron density.

Year	Latitude	Day Max	Season (Month)	Day Min	Season (Month)	Night Max	Season (Month)	Night Min	Season (Month)
2010	90	3524.6	Summer (Jul)	2563.1	Winter (Jan)	3045.9	Summer (Jul)	2143.2	Winter (Jan)
	45	3082.1	Winter (Jan)	2586.5	Spring (Apr)	1701.4	Summer (Jul)	1532.6	Winter (Jan)
	0	2307.5	Summer (Jul)	2009.5	Spring (Mar)	1242.9	Winter (Jan)	1191	Spring (Apr)
	-45	3068.9	Summer (Jul)	2647.7	Spring (Apr)	1775.1	Winter (Jan)	1597.8	Summer (Jul)
	-90	3536.6	Winter (Jan)	2569.4	Summer (Jul)	3028.6	Winter (Jan)	2140.2	Summer (Jul)
2011	90	3524.6	Summer (Jul)	2656.3	Winter (Jan)	3046	Summer (Jul)	2143.2	Winter (Jan)
	45	3082.1	Winter (Jan)	2586.3	Fall (Oct)	1699.7	Summer (Jul)	1532.3	Winter (Jan)
	0	2309.4	Summer (Jul)	2010.4	Spring (Mar)	1241.3	Winter (Jan)	1189.2	Spring (Mar)
	-45	3068.6	Summer (Jul)	2629.5	Fall (Oct)	1775.6	Winter (Jan)	1598.7	Summer (Jul)
	-90	3536.8	Winter (Jan)	2569.5	Summer (Jul)	3028.5	Winter (Jan)	2140.2	Summer (Jul)
2012	90	3523.6	Summer (Jul)	2563	Winter (Jan)	3042.3	Summer (Jul)	2143.1	Winter (Jan)
	45	3082.2	Winter (Jan)	2593.4	Fall (Oct)	1697.3	Summer (Jul)	1532	Winter (Jan)
	0	2306.9	Summer (Jul)	1990.5	Fall (Oct)	1240.1	Winter (Jan)	1188	Spring (Apr)
	-45	3062.3	Summer (Jul)	2636.4	Fall (Oct)	1775.4	Winter (Jan)	1601	Summer (Jul)
	-90	3536.9	Winter (Jan)	2580.3	Summer (Jul)	3027.8	Winter (Jan)	2147.4	Summer (Jul)

Table 4.1: Space Plasma Electron Temperature (K)

Year	Latitude	Day Max	Season (Month)	Day Min	Season (Month)	Night Max	Season (Month)	Night Min	Season (Month)
2010	90	2226.2	Winter (Jan & De	1497.2	Multiple	2197.5	Winter (Dec)	1497.2	Multiple
	45	1949.6	Winter (Jan)	1946.6	Winter (Jan)	1538.1	Summer (Jul)	1064.9	Winter (Jan)
	0	1628.2	Winter (Jan)	1628.1	Fall (Sep)	924.3	Spring (Mar)	924.3	Spring (Mar)
	-45	1936.1	Winter (Jan)	1932.9	Summer (Jul)	1500	Winter (Jan)	1002	Summer (Jul)
	-90	2226.2	Summer (Jun & J	1497.2	Multiple	2198.4	Summer (Jun)	1497.2	Multiple
2011	90	2226.1	Winter (Jan & De	1497.2	Multiple	2197.4	Winter (Dec)	1497.1	Multiple
	45	1949.6	Summer (Jun)	1946.6	Winter (Jan)	1538.1	Summer (Jul)	1064.7	Winter (Jan)
	0	1628.2	Winter (Jan)	1628.1	Multiple	939.6	Fall (Nov)	924.3	Spring (Mar)
	-45	1936.2	Winter (Jan)	1933	Summer (Jul)	1500.1	Winter (Jan)	1002.2	Summer (Jul)
	-90	2226.1	Summer (Jun & J	1497.1	Multiple	2198.4	Summer (Jun)	1497.1	Multiple
2012	90	2226.1	Winter (Jan & De	1497.1	Multiple	2190.3	Winter (Dec)	1497.1	Multiple
	45	1949.6	Summer (Jun)	1946.5	Winter (Jan)	1532.4	Summer (Jul)	1064.5	Winter (Jan)
	0	1628.2	Winter (Jan)	1628.1	Multiple	939.7	Fall (Nov)	924.3	Spring (Mar)
	-45	1936.3	Winter (Jan)	1933.1	Fall (Sep)	1502.2	Winter (Dec)	1002.4	Summer (Jul)
	-90	2226.1	Summer (Jun & J	1497.1	Multiple	2191.5	Summer (Jun)	1497.1	Multiple

Table 4.2: Space Plasma Ion Temperature (K)

Year	Latitude	Day Max 10^(11)	Season (Month)	Day Min 10^(11)	Season (Month)	Night Max 10^(11)	Season (Month)	Night Min 10^(11)	Season (Month)
2010	90	0.32251	Summer (Aug)	0.11948	Winter (Feb)	0.37587	Summer (Aug)	0.11969	Winter (Feb)
	45	0.74177	Fall (Nov)	0.23969	Winter (Jan)	0.33128	Fall (Oct)	0.096929	Winter (Jan)
	0	2.0568	Fall (Nov)	0.98596	Summer (Jul)	0.83811	Fall (Nov)	0.17161	Summer (Jul)
	-45	0.94962	Fall (Nov)	0.37566	Summer (Jul)	0.43342	Winter (Dec)	0.068269	Summer (Jul)
	-90	0.27207	Winter(Dec)	0.099707	Summer (Aug)	0.28639	Winter (Dec)	0.1329	Summer (Aug)
2011	90	0.55423	Fall (Nov)	0.25292	Winter (Jan)	0.588	Summer (Aug)	0.26617	Winter (Jan)
	45	1.4561	Fall (Nov)	0.67718	Winter (Jan)	0.72973	Summer (Jun)	0.19147	Winter (Jan)
	0	2.9679	Fall (Nov)	1.699	Summer (Jul)	1.516	Fall (Nov)	0.53969	Summer (Jul)
	-45	1.7135	Fall (Oct)	0.80557	Summer (Jul)	0.75944	Winter (Dec)	0.086261	Summer (Jul)
	-90	0.54753	Fall (Oct)	0.2617	Summer (Jul)	0.56644	Fall (Sep)	0.29294	Winter (Jan)
2012	90	0.64677	Fall (Nov)	0.42238	Winter (Jan)	0.72384	Spring (May)	0.45039	Winter (Jan)
	45	1.7046	Fall (Nov)	1.0822	Summer (Jul)	0.97328	Summer (Jun)	0.31426	Winter (Jan)
	0	3.3623	Fall (Nov)	2.1111	Summer (Jul)	1.7299	Fall (Nov)	0.75366	Summer (Jul)
	-45	2.0329	Fall (Oct)	1.0394	Summer (Jul)	0.87106	Winter (Dec)	0.098977	Summer (Jul)
	-90	0.68448	Fall (Oct)	0.33259	Summer (Jul)	0.3901	Winter (Feb)	0.3901	Winter (Feb)

Table 4.3: Space Plasma Electron Number Densities (particles/m^3)

Using the maximum energy levels during night and day conditions charging analysis was performed using SPIS. The maximum day electron temperature was found to be 3536.9 K during 2012 at latitude of -90 degrees; this corresponds with T_i = 2226.1 K and $N_i = 0.684 \cdot 10^{11}$ m^{-3}. The minimum day electron temperature is 1990.5 K at 0 degrees latitude in 2012, which corresponds to ion temperature of 1628.1 K and density of $2.111 \cdot 10^{11}$ m^{-3}. The maximum night electron temperature was found to be 3046 K at 90 degrees latitude in 2011, corresponding to 2197.4 K

ion temperature and $0.588 \cdot 10^{11}$ m^{-3}. The minimum night electron temperature was found to be 1188 K at 0 degrees latitude in 2012; corresponding to an ion temperature of 924.3 K and a density of $0.75366 \cdot 10^{11}$ m^{-3}. These values are used in SPIS to find the maximum and minimum charging conditions in night and day of a 3 unit configuration.

The sunspot number used was 400, the maximum allowable by the IRI model. The altitude and other orbital parameters remained the same from the normal environment. The outputs showed a maximum energy of electrons of 3536.9 K with a number density of 0.3520E11 electrons per cubic meter, the respective ions have 1804.1 K and $0.35979 \cdot 10^{9}$ m^{-3}. The minimum levels found were to be 2094.6 K for electrons corresponding to 1190.8 K for ions with number densities of $7.38 \cdot 10^{9}$ and $5.97 \cdot 10^{9}$ m^{-3} respectively. The summary of these values is seen in Table 4.4 for both 2011 and 2012.

Year		*Electron Temp, K*	*Ion Temp, K*	*Electron Density, m^-3*	*Ion Density, m^-3*
2011	Max	3536.9	1804.1	3.52E+10	3.60E+08
	Min	2094.6	1190.8	7.38E+09	5.97E+10
2012	Max	3211.8	2253.2	3.68E+10	1.78E+10
	Min	2189.8	1527.3	3.05E+10	2.30E+09

Table 4.4: IRI Model Storm Data Summary

4.1.3: Spacecraft Charging Simulation Results

The SPIS simulations for the nominal input conditions show that the maximum daytime charging to result in a potential of 0.763 V and 0.802 V for the 2 and 3 unit configurations respectively. The minimum day charging was found to be -0.655 V and -0.732 V for 2 and 3 units respectively. The maximum night charging was found to be 0.445 and 0.489 volts for the 2 and 3 units respectively. The minimum night charging on the CubeSat was found to be -0.306

and -0.277 V for the 2 and 3 units respectively. Table 4.5 has the summary of the results for a three unit CubeSat, and a three-dimensional plot is shown in Figure 4.5.

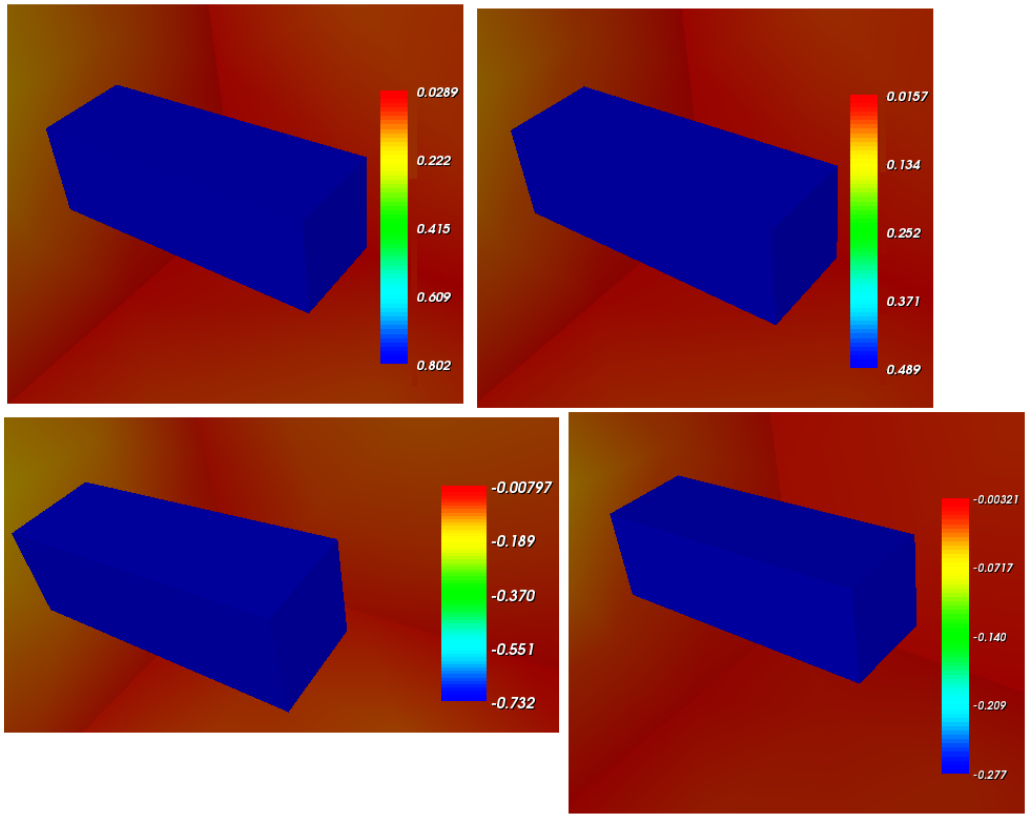

Figure 4.5: Spacecraft Charging (V) for 3 Unit Configuration for Maximum Day (top left), Maximum Night (top right), Minimum Day (bottom left) and Minimum Night (bottom right)

Configuration	Day Max (Volts)	Day Min (Volts)	Night Max (Volts)	Night Min (Volts)
3 Unit	0.802	0.489	-0.732	-0.277

Table 4.5: Summary of the Charging Analysis Results from SPIS

In addition to the expected space weather conditions predicted, magnetic storm data was also extracted from the IRI model by modifying the solar activity index. The corresponding data was analyzed for maxima in order to find conditions the CubeSat would likely encounter should a magnetic storm occur during its flight operations.

Using the data from Table 4.13, the data was input into SPIS, with the results shown in Figure 4.6. The maximum and minimum daytime charging during simulated magnetic storm conditions was found to be 11.3 V and 8.22 V respectively for the 3 unit configuration. The maximum and minimum nighttime charging analysis found -4.32 V and -2.48 V for the magnetic storm conditions as output by the IRI model and simulated on a 3 unit configuration in SPIS.

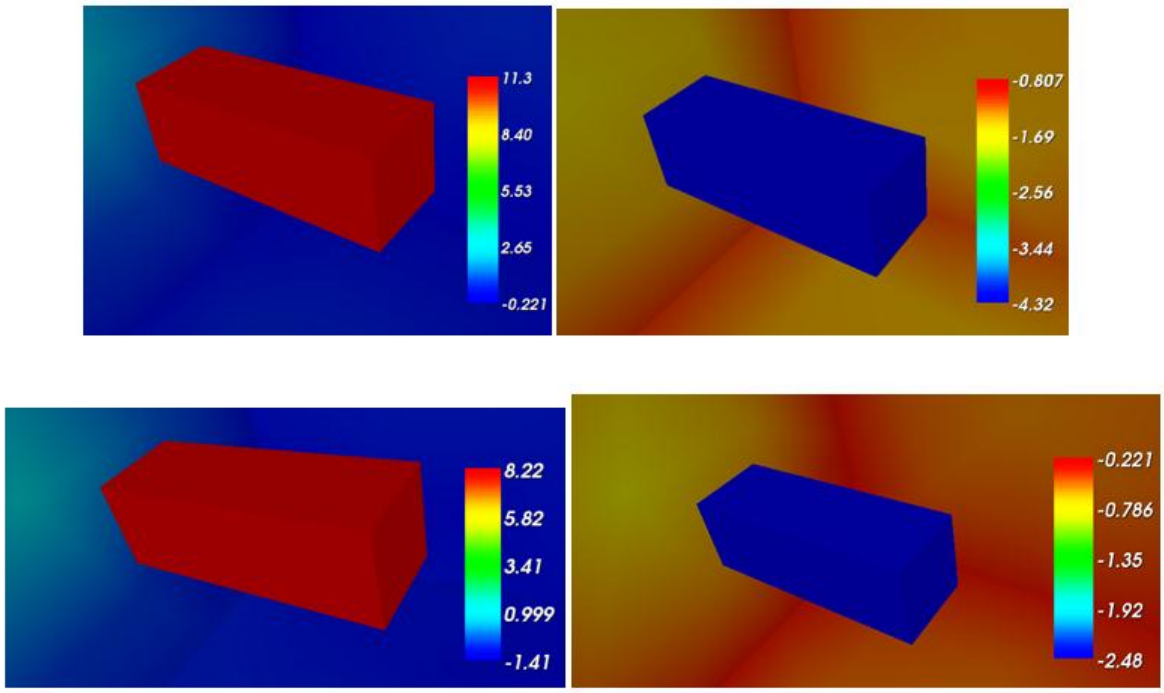

Figure 4.6: Maximum Day/Night Spacecraft Charging (top left/night) and Minimum Day/Night Charging (bottom left/right) During a Magnetic Storm

4.2: Electromagnetic Interference Analysis

In many space missions, knowledge of the ambient magnetic field (MF) can be used for control, or science objectives attitude determination. Electromagnetic interference (EMI) is an

important part of mission design. Many electronics and other subsystem components onboard the spacecraft emit electromagnetic radiation that can interact with other components, or impact the ambient electromagnetic environment in the vicinity of the spacecraft. If these alterations to the natural ambient magnetic field are not taken into consideration valuable data from the MF lines can be lost or too corrupted for use, rending any components which use the MF readings useless. Many basic software physics engines employ a magnetic field solver as part of a basic package in electromagnetism. Specifically, here we are interested in only the magnetic field. Input parameters can be determined by specific components that are analyzed, many parameters are given in a spec sheet from the manufacturer.[35]

The objectives of this EMI analysis were to determine the impact of the solenoid valves used in the propulsion subsystem on the readings of a magnetometer onboard the CubeSat and to establish a location with minimal EMI to place a magnetometer.

4.2.1: Modeling of Induced Magnetic Fields

First, we consider only a stationary situation where all the solenoid valves are on simultaneously. This situation is known as 'magnetostatic,' meaning the MF is not changing in time. Following, we can use the special case of Ampere's Law where there is no time dependence, shown in Equation 4.4.[33]

$$\nabla \times H = J \qquad (Eq. 4.4)$$

Here, H is the magnetic H-field (A/m), J is the current density (A/m^2), and $\nabla \times$ is the curl operator. Qualitatively speaking, Equation 4.15 states that a current passing through a conducting material generates a magnetic field. Next, we substitute in for J as shown in Equation 4.5.

$$J = \sigma v B + J_e \qquad (Eq. 4.5)$$

Here, σ is electric conductivity (S/m), *v* the velocity of the conductor (m/s), B the magnetic B-field (A/m^2), and J_e is the external current density (A/m^2). Now, using the definition of the magnetic potential, we arrive at the Equation 4.6, the equation of magnetostatics.

$$B = \nabla \times A \;\; \& \;\; B = \mu_0 (H + M) \;\Rightarrow\; \nabla \times \left(\mu_0^{-1} \nabla \times A - M \right) - \sigma v \times (\nabla \times A) = J_e \;\; (Eq. 4.6)$$

Here, *M* corresponds to the magnetization (A/m) and the velocity term only applies to axisymmetric and 2 dimensional cases.[34]

Some of the parameters are determined by the geometry or the specific material in question. For instance, the current density is specified by the current total divided by the cross sectional area that it is passing through. Meaning a larger cross section yields a smaller J, while a smaller cross section yields a larger J for the same current. The electrical conductivity is a function of the cross sectional area, the length, and also the resistance which is a property specific to each material and lastly μ_0 is a constant the permeability of a vacuum. Thus, by carefully selecting specific wire geometries and also material the MF can be altered quite dramatically.

4.2.2: EMI Software Evaluation

Due to the other subsystem experience and usage of SolidWorks including thermal calculations and structural analysis, SolidWorks was the first candidate for EMI analysis. By doing so it would help ease the flow of information between subsystems, the same SolidWorks model could be shared between multiple subsystems while operating multiple modules in order

to evaluate a particular scenario. SolidWorks by default does not have a module for EMI, so we decided not to use SolidWorks for EMI analysis.

Other software considered includes ANSYS and COMSOL. ANSYS while extremely powerful and useful is complicated and outside the time constrains of this project. COMSOL on the other hand is with its streamlined programming and intuitive steps are better suited for our project. COMSOL also has the ability to import SolidWorks models. This allows the user to change a particular parameter either in SolidWorks or in COMSOL and the other program will be automatically updated. However, the models from SolidWorks may be too detailed and the required mesh grid can be extremely complex and likely take up most of the memory allotted to the program by the computer. As a result, the user must manually clean up the SolidWorks mesh before it can be used to its full extent within COMSOL. COMSOL can also directly import SolidWorks models by reading a different file format; but the same problem persists within the mesh grid. COMSOL also contained an AC/DC module with a specific component geared for magnetic field analysis. Ultimately, COMSOL was chosen for its user friendliness and its default module for EMI analysis.

4.2.3: Expected Environment

Based on the structures subsystem model of the 3U configuration the magnetometer was originally going to be placed inside the CubeSat for analysis. The magnetometer measure the MF and based on that information it determines position and based on these readings when to turn on or off a magnetorquer for attitude control. The propulsion subsystem team has solenoid valves inside a stainless steel casing. A specifications sheet (Appendix B) with specific values for power and voltage were given. Based on the manufacturer's specifications sheet listing the wire

as 24 American Wire Gage, it was found to be operating at a voltage of 5 V and a power of 0.65 W. This implies a current of 0.13 A in the wire. The American Wire Gage lists its cross sectional area for the 24 as 0.205 mm^2, giving a current density of 0.6341 A/mm^2 (634100 A/m^2).

The 3U CubeSat was modeled using the basic structural interface in COMSOL. Due to the program's relatively simple structural interface, the solenoid was approximated by a series of cylindrical shells placed in series, as seen in Figure 4.7.

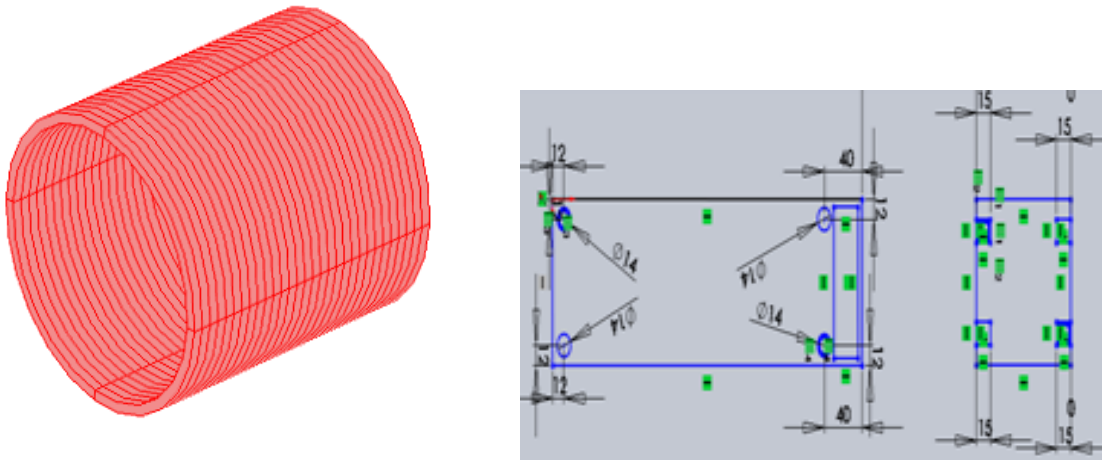

Figure 4.7: Cylindrical Shells Approximating a Solenoid and Flight Option Schematic

Four of these solenoids were placed in their proper location according to a 3U configuration schematic of the flight option provided by the structures subsystem and assigned a copper composition, also seen in Figure 4.18. Based on the number of turns per unit length it was determined that 30 turns would be inside the solenoid, as such 30 cylinders were created to model the solenoid. The magnetic field modeled was in 3 dimensions around the outside of the solenoids, which includes the internal part of the CubeSat as well as an external volume outside the CubeSat. For analysis purposes, we considered a possible boom option at 10, 20 and 30 cm from the end of the CubeSat in both along the length of the CubeSat and perpendicular. This was

done in case a boom was chosen, it could be oriented on any face of the cube at varying lengths and our analysis would still have results for that distance away from the CubeSat at a particular orientation.

In order to evaluate a worst case type scenario, no metal casing was placed over the outside of the solenoid. With this, it would be the maximum MF that could be produced by our model. The solenoids were placed inside an aluminum box in the configuration of a 3U volume with a thickness of 4mm to simulate the body of the CubeSat. A larger volume of 1 m^3 of empty space was created to simulate the immediate vicinity of the CubeSat for magnetic field analysis.

4.2.4: EMI Results

The results for a 3U CubeSat with a 10, 20 and 30 cm boom aligned with the long axis of the CubeSat are shown in Figures 4.8, 4.9, and 4.10 respectively.

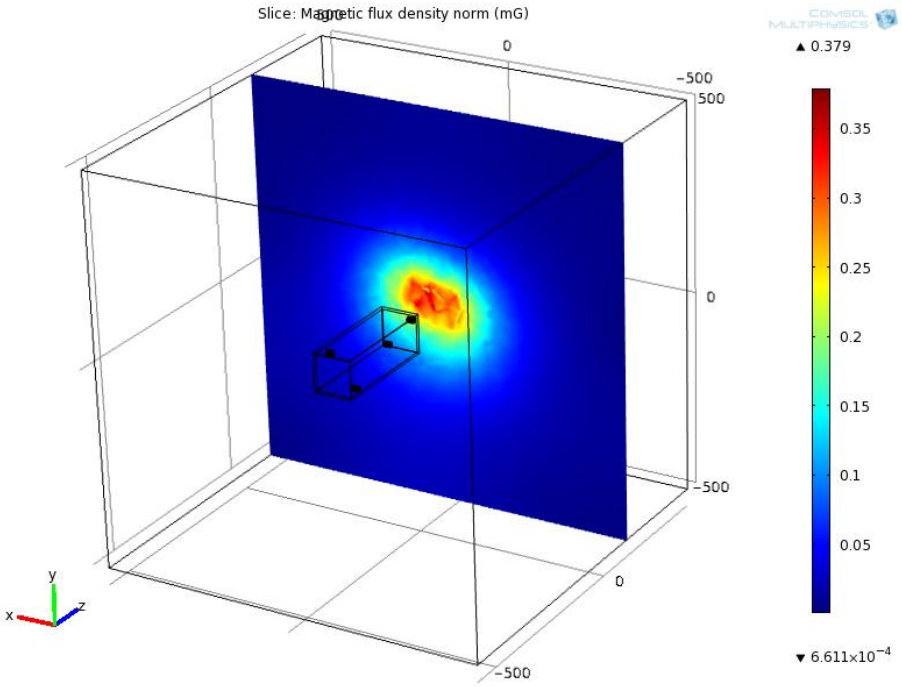

Figure 4.8: Magnetometer Placement on 10 cm Boom Aligned with the CubeSat

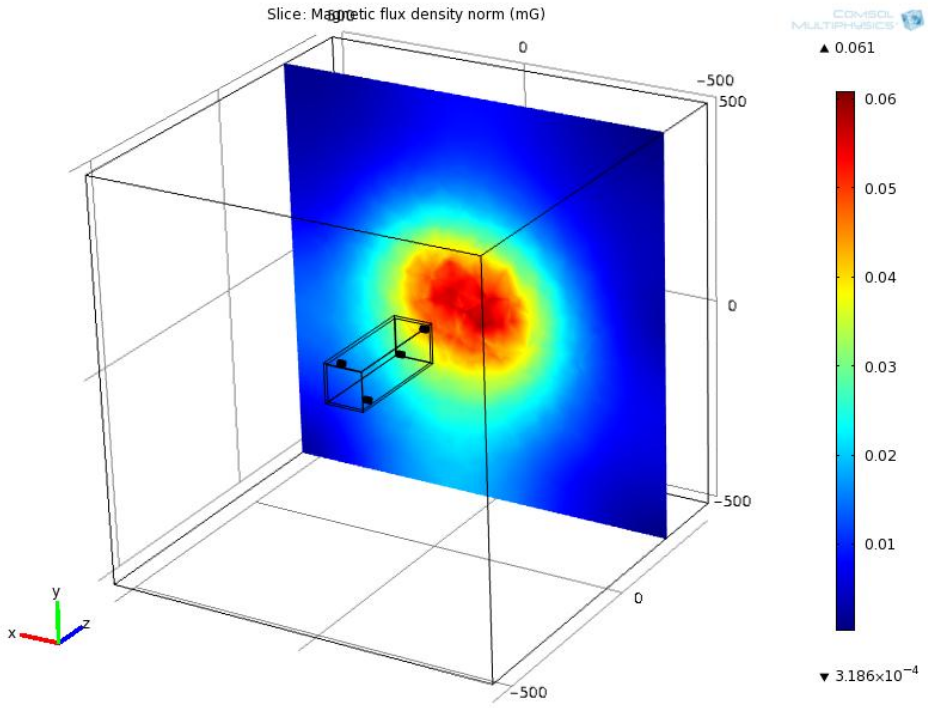

Figure 4.9: Magnetometer Placement on 20 cm Boom Aligned with the CubeSat

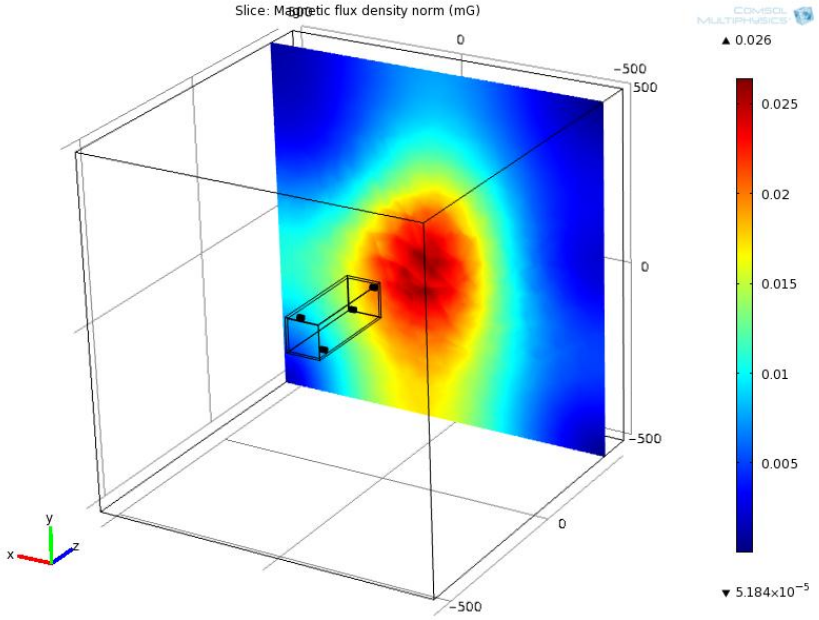

Figure 4.10: Magnetometer Placement on 30 cm Boom Aligned with the CubeSat

The results plotted in Figures 4.11 through 4.13 show another possible consideration, placing the boom perpendicular to the CubeSat's long axis. This possible configuration would depend on how the boom would want to be deployed and other structural concerns as to whether or not it would be aligned or perpendicular to the long axis of the CubeSat, the 10, 20, and 30 cm boom results are located in Figures 4.11, 4.12 and 4.13 respectively.

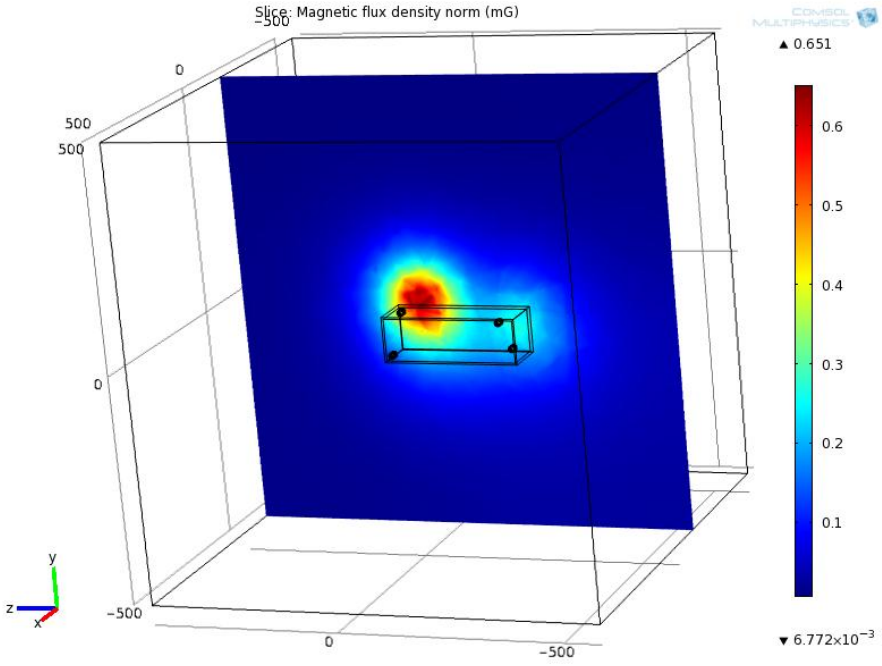

Figure 4.11: Magnetometer Placement on 10cm Perpendicular Boom

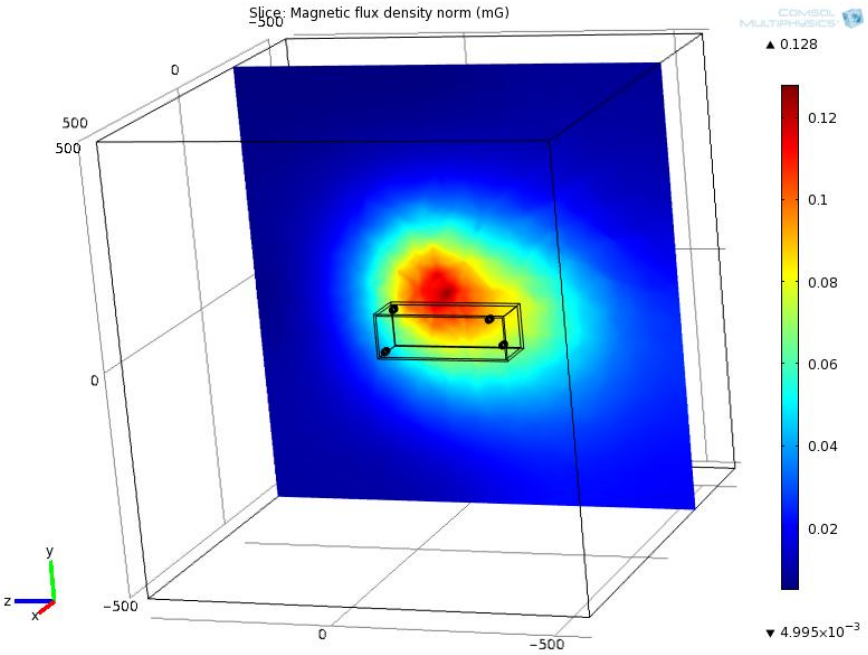

Figure 4.12: Magnetometer Placement on 20cm Perpendicular Boom

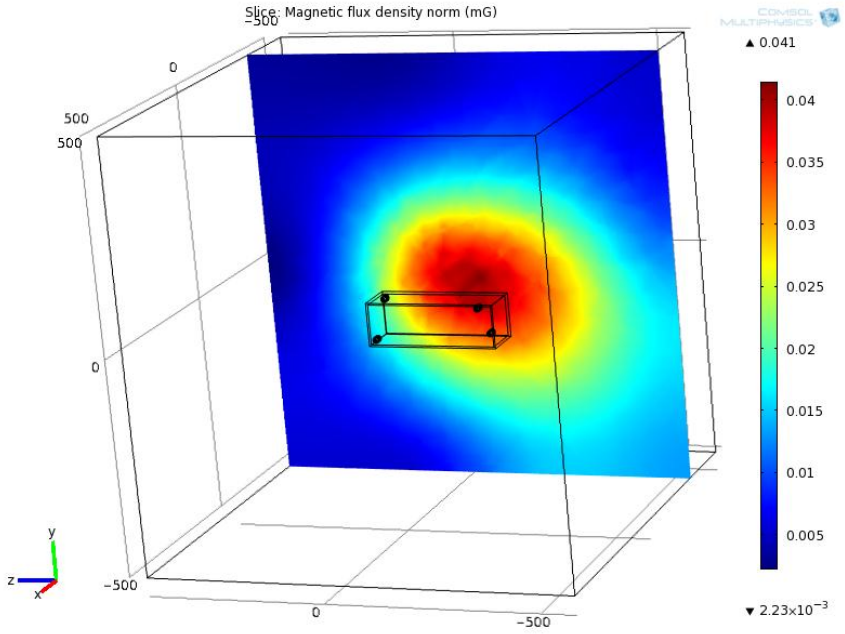

Figure 4.13: Magnetometer Placement on 30cm Perpendicular Boom

Chapter 5: Magnetometer Design

Magnetometers are used to measure the magnitude and direction of the local magnetic field around the spacecraft during flight operations. They are commonly implemented on satellites in LEO for use in the ADCS and payload subsystems. At LEO altitudes the magnetic field of the Earth is relatively strong, ranging from approximately 0.3 to 0.6 gauss depending on the location of the satellite. Using computational modeling of the expected magnetic field, the satellite's ADCS can use readings from the magnetometer to determine the location of the spacecraft by comparing the measured magnetic field to the models stored in the OBC. Additionally, magnetometer usage is often driven by the payload and science requirements. In the case of polar-orbiting missions that operate where the Earth's magnetic field is at its strongest, precise magnetic field measurements and calculations may be critical to the operation and accuracy of the instrument.

Our CubeSat will be using an ADCS that will rely partially on magnetorquers to orient itself with respect to the Earth's magnetic field, the fidelity of the magnetometer's measurements are critical to the success of the mission. Thus, there are two primary factors to consider when selecting a magnetometer for the mission. The precision, accuracy, and resolution of the device are one factor; the magnetometer must be able to make correct measurements as often as possible, and require the best possible abilities in these areas. The second factor is disturbances in the magnetometer readings; the spacecraft's electronic components will generate magnetic fields when running which could create electromagnetic interference with the magnetometer's readings and lead to false measurements. For this reason, magnetometers are often extended from the spacecraft on mechanical booms to keep the instrument away from the interference

from the spacecraft. Since our team focused on environmental and electromagnetic effects on the spacecraft, we also selected and designed the magnetometer to be used on our CubeSat.

5.1: Magnetometer Selection

Before selecting our flight option magnetometer, we were given a few specifications by the ADCS team to keep in mind during selection. These specifications, in order of importance, were:

1. The magnetometer is a digital instrument (as opposed to analog)

2. The magnetometer is capable of three-axis measurements

3. The magnetometer operates in 3.3 V (reduces required power conditioning)

4. The magnetometer has its own circuit board (reduces integration work)

With these requirements in mind, the magnetometer we chose was the Honeywell HMC5883L. The HMC5883L is a multi-chip 12 bit three-axis digital magnetic compass designed for low cost magnetometry. Some of the important technical specifications are listed in Table 5.1 below, and an image is shown in Figure 5.1. The full spec sheet is given in the appendix.

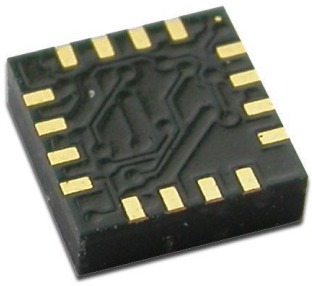

Figure 5.1: Honeywell HMC5883L

Parameter	Value
Supply Voltage (V)	2.16 – 3.60
Average Current Draw (μ A)	2.0 (idle) – 100.0 (measurement mode)
Detection Field Range (Gauss)	± 8.0
Resolution (mGauss)	5.0
Dimensions (mm)	3.0 x 3.0 x 0.9
Mass (mg)	50.0

Table 5.1: Magnetometer Specifications

The HMC5883L meets three of the four specifications asked for by the ADCS team. It is a digital magnetometer, so the ADCS team will not need to convert any analog signals in the OBC from our device. It is a three-axis magnetometer, so we will only need one to enable complete measurements of the magnetic field in orbit. The supply voltage range includes the nominal 3.3 Volts that will be the standard on our CubeSat. Unfortunately, the magnetometer does not come with its own PCB attached, so we will have to select a board to mount it on. The magnetometer itself is quite small, both in weight and dimension, so finding a circuit board to mount it on that complies with our limited mass budget should be fairly easy. Honeywell sells test boards specifically for their HMC series digital compasses, but none are space qualified. Based on these test boards, we estimate that the total mass of the magnetometer, the PCB needed to connect it to the OBC, and the casing to enclose the device will be around 5 grams in mass.

5.2: Magnetometer Boom Design

The mass estimate for our magnetometer package allowed us to proceed with designing a deployable boom for our instrument. There are two main types of deployable booms; telescopic and spring-loaded. Telescopic booms collapse in a series of shells like a looking glass telescope. This allows the boom to be stowed in a small volume within the satellite during launch and before deployment. Telescopic booms are mechanically more complex than spring-loaded booms. Spring-loaded booms are typically not collapsible, but instead are stowed on the side of the spacecraft in their full-length configuration, and are deployed by a spring-like mechanism after launch. Spring-loaded booms are simpler mechanically than telescopic booms, but are limited in length by the length of the spacecraft itself. Because of the restrictive mass and power budget of our CubeSat, we decided to employ a spring-loaded boom that can be stowed on the side of our CubeSat. After consulting with the structures subsystem team, we found that the CubeSat regulations allow protrusions outside the outer walls of the CubeSat of up to 6 mm in thickness. This relaxation of dimension allows for external instruments, such as protruding camera lenses or deploying booms. Thus, our design constraint was to limit the thickness of our boom to approximately 5.5 mm to allow for a contingency factor. Additionally, this limiting thickness, coupled with the simplicity of our boom, required that the wires connecting the magnetometer PCB to the internal OBC must be secured to the boom, not stowed within an opening inside of it. The boom can be secured using thin pieces of plastic wire or fishing line attached to a series of resistors. When the boom is ready to be deployed, the OBC calls for power to be sent through the attached resistors. The heat melts the plastic wire, which snaps, allowing the secured spring-loaded beam to deploy. Similar mechanisms are used for the deployment of the CubeSat antennae.

The biggest concern for us during our beam design was the vibration of the beam due to disturbances after it is deployed. Large vibrations potentially could lead to large displacements of our instrument, which in turn will create a moment of inertia that is un-accounted for by our ADCS algorithms. Therefore, we would like the fundamental frequency of our boom to be relatively high, as this will generally lead to a smaller maximum displacement during vibration.

To find the natural frequency of vibration of our boom, we considered it as a simple, undamped, single degree of freedom oscillator.[37] The natural frequency of such a system is given by Equation 5.1.

$$f_n = \frac{1}{2\pi}\sqrt{\frac{k}{m}} \qquad (Eq\ 5.1)$$

Here, *k* is the stiffness of the boom, and *m* is the effective mass. To find these properties, we need to know more of our boom parameters.

We chose to construct the boom out of Aluminum 7075, a common Aluminum alloy used in CubeSat applications. Our boom will be 5.5 mm thick, and will be circular in cross-section. Our EMI analysis showed that a 10 cm boom will keep the magnetometer at a safe distance from the CubeSat body, so we will set our boom length to 10 cm in accordance. The resulting boom parameters are shown in Table 5.2.

Parameter	Value
Material	Aluminum 7075
Density (kg/m^3)	2810
Elastic Modulus (GPa)	69.0
Diameter (mm)	5.50
Length (cm)	10.0
Cross-Sectional Area (mm^2)	23.76
Volume (mm^3)	2375.83
Boom Mass (g)	6.676

Table 5.2: Magnetometer Boom Parameters

With these parameters, we can find both the stiffness of the boom and the equivalent mass of the boom-magnetometer system. The stiffness of the boom is described by Equation 5.2.

$$k = \frac{AE}{L} \qquad (Eq. 5.2)$$

Here, A is the cross-sectional area, E is the elastic modulus, and L is the boom length. Using Equation 5.2, the stiffness of our boom is calculated to be 16.39 MN/m. The equivalent mass of the boom can be described by Equation 5.3.

$$m_{eq} = M_{magnetometer} + 0.23 m_{boom} \qquad (Eq. 5.3)$$

We find that the equivalent mass of our oscillating system is 6.54 g. Finally, we can solve for the fundamental frequency of vibration of our boom using Equation 5.1. The result is a fundamental frequency of vibration of 7.97 kHz. This high frequency of vibration, coupled with our expectation of small perturbing forces, indicates that our boom will not be greatly displaced during flight.

Chapter 6: Conclusions and Recommendations

Based on previous CubeSat mission profiles, we conclude that our proposed Argus Infrared Spectrometer payload is a suitable payload for our first CubeSat design. This choice of scientific payload will allow all subsystem teams to exercise their knowledge of spacecraft design around a relatively simple payload. The AIRS is easily integrated within a 3U CubeSat, and can perform a variety of interesting scientific experiments.

After collecting the survival and operating temperature ranges from the other subsystem team, we concluded that the CubeSat must be kept within a temperature range of 0°C to 50°C at all times.

Hot and cold case thermal simulations resulted in predicted maximum and minimum temperature limits. The maximum temperatures for our CubeSat were calculated to be -23.9°C for the cold-case and 31.6°C for the hot-case.

Based on these conclusions, it is recommended that the CubeSat be coated in black paint due to its thermal properties. The black paint coating should be supplemented by interior sheets of multi-layer insulation to reduce heat loss during the eclipse period and keep the CubeSat within the allowable temperature limits.

The maximum magnitude voltages predicted on the surface of the 3U CubeSat are -0.732 V (night) and 0.802 (day). The minimum voltages are -0.277 V (night) and 0.489 V (day). Based on the analysis and numerical data from SPIS, we can conclude that the nominal environment spacecraft charging will not be an issue during the mission lifetime.

During the magnetic storm, the developed voltage magnitudes increased to 11.3 V (day) and -4.32 V (night). The minimum voltages during the magnetic storm were 8.22 V (day) and -2.48 V (night). Although the voltages here have significantly increased due to storm conditions, charging still should not cause any serious damage or impede operations of the CubeSat.

Based on the relative magnitudes of the magnetic field at the end of the CubeSat, it was recommended that a boom be used for the magnetometer to minimize the solenoids' contributions to the measureable magnetic field and allow for more accurate and precise readings from the magnetometer. The magnitude of the magnetic field at the locations perpendicular to the long axis of the CubeSat was found to be roughly ~10^{-4} G (~0.1 mG), while aligning the boom with the long axis reduced the electromagnetic interference due to the solenoids by between 2 and 4 orders of magnitude depending on length of the boom. The chosen magnetometer's overall saturation limit is ±8 Gauss, and is sensitive up to the level of 5 mG. Based on the analysis, it is recommended that we minimize the electromagnetic interference from the solenoids by placing the magnetometer on a boom of at least 10 cm long, if not more, and have it be aligned with the long axis of the 3U configuration CubeSat in order to further minimize the magnetic field induced by the solenoid valves.

Based on our EMI analysis, a 10 cm boom protruding from the long-axis side will allow the magnetometer to operate free of any interference effects. A spring-loaded boom is recommended to limit power requirements and to allow the boom to be surface mounted, instead of stowed inside the CubeSat. Additionally, a 5.5 mm diameter circular boom will be stiff enough to reduce large displacements during vibrations caused by external forces after deployment.

References

[1] “CubeSat Mission Statement." *CubeSat.org*. Web. 26 Feb. 2011. <http://www.cubesat.org/index.php/about-us/mission-statement>.

[2] AAU CubeSat. Digital image. *AAU CubeSat - Student Satellite*. Aalborg University. Web. 26 Feb. 2011. <http://www.cubesat.auc.dk/pictures/AAUcubesat.jpg>.

[3] AAUSAT Camera Mount and Lens. Digital image. *AAU CubeSat - Student Satellite*. Aalborg University. Web. 26 Feb. 2011. <http://cubesat.aau.dk/pictures/lcto/pls.jpg>.

[4] AAUSAT-II. Digital image. *AAUSAT-II Launch Info*. Aalborg University. Web. 26 Feb. 2011. <http://aausatii.space.aau.dk/pictures/integration/slides/200705041644520.html>.

[5] Aerocube 3. Digital image. *Headlines*. The Aerospace Corporation. Web. 26 Feb. 2011. <http://www.aero.org/publications/crosslink/summer2009/headlines.html>.

[6] Stras, Luke, Daniel D. Kekez, G. James Wells, Tiger Jeans, Robert E. Zee, Freddy Pranajaya, and Daniel Foisy. "The Design and Operation of The Canadian Advanced Nanospace EXperiment (CanX-1)." Web. 26 Feb. 2011. < http://www.utias-sfl.net/docs/canx1-amsat-2003.pdf>

[7] CanX-2. Digital image. *Mike Rupprecht - Amateur Radio*. Web. 26 Feb. 2011. <http://www.dk3wn.info/images/canx2.jpg>.

[8] “Canadian Advanced Nanospace eXperiment 2: Scientific and Technological Innovation on a Three-Kilogram Satellite,” Karan Sarda, Stuart Ealeson, Eric Caillibot, Cordell Grant, Daniel Kekez, Freddy Pranajaya, Robert E. Zee, Acta Astronautica 59 (2006) pp. 236 – 245.

[9] Compass-1. Digital image. *COMPASS 1 Cubesat Project*. Web. 23 Feb 2011. <http://www.raumfahrt.fh-aachen.de/compass-1/home.htm>.

[10] CP6. Digital image. *PolySat*. Web. 23 Feb 2011. <http://polysat.calpoly.edu/CP6.php>.

[11] "Cute-1.7+ADP II M." *Cute-1.7+ADP II*. Web. 23 Feb 2011. <http://lss.mes.titech.ac.jp/ssp/cute1.7/index_e.html>.

[12] Delfi-C3. Digital image. AMSAT - The Radio AMateur Satellite Corporation. Web. 26 Feb. 2011. <http://www.amsat.org/amsat-new/satellites/photos/delfi-c3.jpg>.

[13] GeneSat-1. Digital image. *Gunter's Space Page*. Web. 26 Feb. 2011. <http://www.skyrocket.de/space/img_sat/genesat-1__1.jpg>.

[14] GeneSat-1 Payload Assembly. Digital image. *NASA- GeneSat-1 Payload Assembly*. NASA. Web. 26 Feb. 2011. http://www.nasa.gov/centers/ames/multimedia/images/2006/genesat_payload_iotd.html

[15] HawkSat-1 CubeSat. Digital image. *CubeSat Kit - In Space*. Web. 26 Feb. 2011. <http://www.cubesatkit.com/images/HawkSat-1.jpg>.

[16] ION CubeSat. Digital image. *University of Illinois- ION Cubesat Project*. Web. 23 Feb 2011. <http://cubesat.ece.illinois.edu/>.

[17] MAST CubeSats. Digital image. Web. 26 Feb. 2011. <http://gallery.ejwassoc.com/uploads/MAST_experiment.jpg>.

[18] MAST Deployed. Digital image. *Gunter's Space Page*. Web. 26 Feb. 2011. <http://www.skyrocket.de/space/doc_sdat/mast.htm>.

[19] "The Norwegian Satellite nCUBE2.." *nCube (Satellite)-Wikipedia*. Web. 23 Feb 2011. <http://en.wikipedia.org/wiki/NCube_%28satellite%29>.

[20] PharmaSat. Digital image. NASA. Web. 26 Feb. 2011. <http://www.nasa.gov/images/content/330070main_PreSat_Assembly_428-321.jpg>.

[21] Long, Matthew, Allen Lorenz, Greg Rodgers, Eric Tapio, Glenn Tran, Keoki Jackson, and Robert Twiggs. "A CubeSat Derived Design for a Unique Academic Research Mission in Earthquake Signature Detection." Web. 26 Feb. 2011. <www.quakefinder.com/research/pdf/SSC_PAPER_SSC02-IX-6.pdf>.

[22] Noca, Muriel, Fabien Jordan, Nicolas Steiner, Ted Choueiri, Florian George, Guillaume Roethlisberger, Noemy Scheidegger, Herve Peter-Contesse, and Maurice Borgeaud. "Lessons Learned from the First Swiss Pico-Satellite: SwissCube." Web. 26 Feb. 2011. <http://ctsgepc7.epfl.ch/12%20-%20SwissCube%20papers/S3-D-SET-1-5-Small%20Sat%2009%20paper%20SSC09-XII-9.pdf>.

[23] "Past Launches." *CubeSat*. CubeSat.org, 2011. Web. 23 Feb 2011. <http://www.cubesat.org/index.php/missions/past-launches>.

[24] Wertz, James R., and Wiley J. Larson, eds. *Space Mission Analysis and Design.* 3rd ed. Hawthorne, CA: Microcosm, 1999. Print.

[25] Incropera, Frank P., David P. DeWitt, Theodore L. Bergman, and Adrienne S. Lavine. *Fundamentals of Heat and Mass Transfer.* 6th ed. Hoboken, NJ: John Wiley & Sons, 2007. Print.

[26] Prof. Pui-Suari, Jordi. Prof. Twiggs, Bob. Munakata, Riki. “CubeSat.” N.p., 02 Sep 2010. Web. 20 Oct 2010. http://www.cubesat.org/

[27] Dr. Holbert, Kieth. "Spacecraft Charging." N.p., 19 Jan 2006. Web. 20 Oct 2010. http://holbert.faculty.asu.edu/eee560/spc-chrg.html

[28] Spacecraft Plasma Interaction Network & ONERA/DESP, Artenum and University Paris VII. “SPIS’s HomePage.” N.p., 03 Jun 2010. http://dev.spis.org/projects/spine/home/spis

[29] Bilitza, Dieter. “International Reference Ionosphere.” N.p., 22 Jun 2009. Web. 20 Oct 2010. http://iri.gsfc.nasa.gov/

[30] Ferguson, Dale. Hillard, Barry. United States.“New NASA SEE LEO Spacecraft Charging Design Guidelines – How to Survive in LEO Rather than GEO.” , 2003.Web. 20 Oct 2010.

[31] Ferguson, Dale. United States. “The LEO Spacecraft Charging Design Standard.” Web. 20 Oct 2010.

[32] Reiff, Patricia H. "The Sun-Earth Connection." *Rice Space Institute*. 11 Jan. 1999. Web. 01 Mar. 2011. <http://space.rice.edu/IMAGE/livefrom/sunearth.html>.

[33] Feynman, Richard, Robert Leighton, and Matthew Sands. *The Feynman Lectures on Physics.* 2nd ed. 2nd vol. Reading, Massachusetts: Addison Wesley, 2005. Chapter 2: Magnetostatics. Print.

[34] “Theory for the Magnetic Fields Interface." *COMSOL Multiphysics - Help*. COMSOL Multiphysics, CD.

[35] United States. Assessment and Control of Spacecraft Electromagnetic Interference., 1972. Web. 24 Feb 2011.

http://www.spaceflightnews.net/special/sp8000/archive/00000126/01/sp8092.pdf

[36] United States. *Low Earth Orbit Spacecraft Charging Design Handbook.* , 2007. Web. 24 Feb 2011. standards.nasa.gov/documents/viewdoc/3315626/331562

[37] Rao, Singiresu S. *Mechanical Vibrations*. 4th ed. Upper Saddle River, NJ [u.a.: Prentice Hall, 2004. Print.

[38] "Argus 1000 IR Spectrometer Owner's Manual." Thoth Technology inc, 04/2010. Web. 24 Feb 2011. <http://www.thoth.ca/manuals/Argus%20Owner%27s%20Manual,%20Thoth%20Technology,%20Apr%2010,%20rel%201.pdf>.

[39] Honeywell International Inc. Honeywell International. *3-Axis Digital Compass IC HMC5883L*. Web. 7 Feb. 2011. <http://www.cgs-tech.com/pdf/HMC5883L.pdf>.

[40] Asco. *Asco Valve Series 411 Catalog Page*. Asco. *ASCO Valve*. Web. 1 Mar. 2011. <http://www.ascovalve.com/Common/PDFFiles/Product/411_SeriesR1.pdf>.

[41] "M-Loc MPM GPS Measurement Platform Module for Mobile Products." *M-Loc MPM*. Trimble Navigation Limited, 2001. Web. 24 Feb 2011. <ftp://ftp.trimble.com/pub/sct/embedded/bin/Data%20Sheets/M-Loc%20MPM.pdf>.

Appendix A: Argus 1000 Infrared Spectrometer Partial Spec Sheet [38]

Table 2: Technical Specifications, Argus 1000 Spectrometer

Argus 1000	Specification
1. Type	Grating spectrometer
2. Configuration	Single aperture spectrometer
3. Field of View	0.15° viewing angle around centered camera boresight with 15mm fore-optics
4. Mass	>230 g
5. Accommodation	45 mm x 50 mm x 80 mm
6. Operating Temp.	-20°C to +40°C operating temperature
7. Survival Temp.	-25°C to + 50°C survival temperature
8. Detector	256 element InGaAs diode arrays with Peltier cooler (100 active channels)
9. Grating	300 g/mm
10. Electronics	microprocessor controlled 10-bit ADC with co-adding feature to enhance precision to 13-bit, 3.6-4.2V input rail 250mA-1500mA (375mA typical)
11. Operational Modes	–Continuous cycle, constant integration time with co-adding feature –Adaptive Exposure mode
12. Data Delivery	Fixed length parity striped packets of single or co-added spectra with sequence number, temperature, array temperature and operating parameters
13. Interface	Prime and redundant serial interfaces RS232 protocol
14. Spectral Channels	100 (typical)
15. Integration Time	500 µs to 4.096 sec
16. Handling	Shipped by courier in ruggedized carrying case

7.2 Detector System

A linear gallium arsenide (InGaAs) photodiode array with high-quantum efficiency pixels in the infrared detect radiation emitted for a 1.5 km^2 surface tile that has been divided spectrally by the grating optics. The array is a hybrid InGaAs and CMOS acitve-pixel readout electronics in which the photo-current is buffered, amplified and stored according to an idealised schematic shown in Figure 3.

Appendix B: Magnetometer Partial Spec Sheet [39]

HMC5883L

SPECIFICATIONS (* Tested at 25°C except stated otherwise.)

Characteristics	Conditions*	Min	Typ	Max	Units
Power Supply					
Supply Voltage	VDD Referenced to AGND	2.16		3.6	Volts
	VDDIO Referenced to DGND	1.71	1.8	VDD+0.1	Volts
Average Current Draw	Idle Mode	-	2	-	µA
	Measurement Mode (7.5 Hz ODR; No measurement average, MA1:MA0 = 00) VDD = 2.5V, VDDIO = 1.8V	-	100	-	µA
Performance					
Field Range	Full scale (FS) – total applied field (Typical)	-8		+8	gauss
Mag Dynamic Range	3-bit gain control	±1		±8	gauss
Resolution	VDD=3.0V, GN=2		5		milli-gauss
Linearity	±2.0 gauss input range			0.1	±% FS
Hysteresis	±2.0 gauss input range		±25		ppm
Cross-Axis Sensitivity	Test Conditions: Cross field = 0.5 gauss, Happlied = ±3 gauss		±0.2%		%FS/gauss
Output Rate (ODR)	Continuous Measurment Mode	0.75		75	Hz
	Single Measurement Mode			160	Hz
Measurement Period	From receiving command to data ready		6		msec
Turn-on Time	Ready for I2C commands		200		µs
Gain Tolerance	All gain/dynamic range settings		±5		%
I^2C Address	7-bit address		0x1E		hex
	8-bit read address		0x3D		hex
	8-bit write address		0x3C		hex
I^2C Rate	Controlled by I^2C Master			400	kHz
I^2C Hysteresis	Hysteresis of Schmitt trigger inputs on SCL and SDA - Fall (VDDIO=1.8V)		0.2*VDDIO		Volts
	Rise (VDDIO=1.8V)		0.8*VDDIO		Volts
Self Test	X & Y Axes		±1.16		gauss
	Z Axis		±1.08		
	X & Y Axes (GN=100)		510		LSb
	Z Axis (GN=100)				
General					
ESD Voltage	Human Body Model (all pins)			TBD	Volts
	Machine Model (all pins)			TBD	
Operating Temperature	Ambient	-30		85	°C
Storage Temperature	Ambient, unbiased	-40		125	°C
Reflow Classification	MSL 3, 260 °C Peak Temperature				
Package Size	Length and Width	2.85	3.00	3.15	mm
Package Height		0.8	0.9	1.0	mm

Appendix C: Solenoid Valve Partial Spec Sheet [40]

ASCO

2 and 3-Way Miniature Solenoid Valves

General Service • Manifold & Line Mount

2/2
3/2
SERIES
411

The 411 Series valves are suitable for a wide range of OEM applications where small size, low power, and long life are critical.

- Cycle life in the hundreds of millions
- Corrosion resistant materials of construction
- Manifold mount construction allows for easy assembly
- Lower power consumption offers extended battery life

Construction

Valve Wetted Parts	
Body	PBT
Gaskets	FKM, NBR, EPDM
Bobbin/Core Tube	PBT
Core and Plugnut	400 Series Stainless Steel
Springs	300 Series Stainless Steel

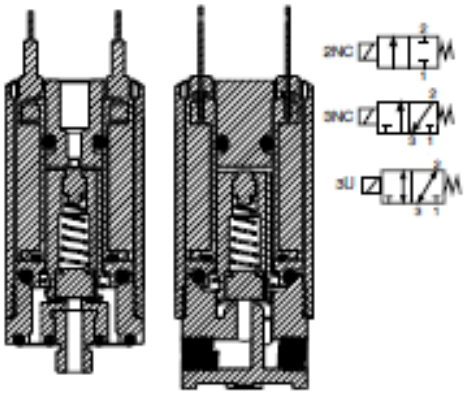

Electrical

Standard Voltages	5VDC, 6VDC, 12VDC, 24VDC
Power Consumption	0.65, 2.0 Watts
Duty Cycle Rating	Continuous
Coil Insulation	266°F (130°C)
Electrical Connection	.110" Spade, 24 AWG Hardwire

Valve

Response Time	~ 10 ms
Internal Volume (Max.)	Line Mount = 620µl Manifold Mount = 564µl
Vacuum Rating	29" Hg
Options	Oxygen clean available 300 Series Stainless Steel Body

Temperature Range:

Ambient & Media:
32°F to 140°F (0°C to 60°C) continuous duty

Approvals:

Consult factory

Alternate Construction/Options

Additional constructions and options are available including alternate elastomers and orifice sizes. Minimum quantities apply. ASCO can also custom design a valve or manifold assembly to your specific application.

Contact your local ASCO sales office for more information

57